공학박사학위논문

Extended theoretical study of E×B flow shear suppression of tokamak turbulence; effects of eddy shape, precession drift shear, and resonant magnetic perturbation

토카막 난류의 ExB 흐름 층밀림 억제의 이론적 확장; 맴돌이 형상, 세차표류 층밀림, 공명자기섭동의 영향

2019 년 2 월

서울대학교 대학원

에너지시스템공학부

최 경 진

공학박사학위논문

Extended theoretical study of E×B flow shear suppression of tokamak turbulence; effects of eddy shape, precession drift shear, and resonant magnetic perturbation

토카막 난류의 ExB 흐름 층밀림 억제의 이론적 확장; 맴돌이 형상, 세차표류 층밀림, 공명자기섭동의 영향

2019 년 2 월

서울대학교 대학원

에너지시스템공학부

최 경 진

Extended theoretical study of E×B flow shear suppression of tokamak turbulence; effects of eddy shape, precession drift shear, and resonant magnetic perturbation

토카막 난류의 ExB 흐름 층밀림 억제의 이론적 확장; 맴돌이 형상, 세차표류 층밀림, 공명자기섭동의 영향

지도교수 함 택 수

이 논문을 공학박사 학위논문으로 제출함

2019 년 1 월

서울대학교 대학원

에너지시스템공학부 원자핵공학전공

최 경 진

최경진의 공학박사 학위논문을 인준함

2018 년 12 월

위 원 장	황용석	(인)
부위원장	함택수	(인)
위 원	나용수	(인)
위 원	이정표	(인)
위 원	고원하	(인)

Abstract

Extended theoretical study of E×B flow shear suppression of tokamak turbulence; effects of eddy shape, precession drift shear, and resonant magnetic perturbation

Gyung Jin Choi
Department of Energy Systems Engineering
The Graduate School
Seoul National University

This thesis aims to extend theory of E×B flow shear induced turbulence suppression to provide explanations to practical issues on transport barrier physics in tokamaks. I extend two-point theory of E×B shear suppression considering tilted turbulence eddies, and identify effect of relative sign of E×B shear and initial tilting on efficiency of turbulence suppression. For trapped electron turbulence, I systematically derive a proper two-point equation, which menifests a synergism between E×B shear and precession shear on turbulence suppression. Finally, I identify resonant magnetic perturbations induced long-term collisionless zonal flow decay by a theoretical study using gyrokinetic equations. I discuss experimental applications and demonstrations of my theoretical works.

Keywords: tokamak, turbulence, E×B flow shear, eddy tilting, magnetic precession drift, resonant magnetic perturbation, gyrokinetics, bounce-kinetics
Student Number: 2012-23288

Contents

Chapter 1

Introduction

Fusion fuels in a tokamak is present as a plasma with very high temperature, and thus with high ionization rate, confined in a strong axisymmetric magnetic field. Since the plasma is hot and the magnetic field is strong enough, typical electrons and ions in the plasma make several gyrations before a collision. The plasma therefore has a strong anisotropy in its physical properties with respect to the magnetic field, i.e., it is magnetized. In theoretical descriptions, tokamak plasmas are often assumed to be fully ionized and strongly magnetized, which is a good approximation for most radial regions except extreme edge. In steady state, a tokamak plasmas satisfies magnetohydrodynamic (MHD) equilibrium $\mathbf{J} \times \mathbf{B} = \boldsymbol{\nabla} P$, so that magnetic field lines in a tokamak plasma configure closed magnetic surfaces, which are basically nested tori. However, perturbations from the equilibrium can raise large-scale MHD instabilities that significantly degrade plasma performance and often lead to a disruption. Therefore, it is necessary to avoid such instabilities, and thus linear stability conditions of

MHD instabilities rule parameter regimes for operation. In the absence of dangerous MHD instabilities, confinement of a tokamak plasma is determined by anomalous transport, of which the rate is usually much higher than that of neoclassical transport by Coulomb collisions. Origin of the anomalous transport is drift-wave-type microscale turbulence. A classic paradigm understanding tokamak turbulence consists of local growth by linear instabilities and saturation by local nonlinear interactions. Here the term local means local in both radial space and **k**-space. Theoretical studies of linear stability conditions have been extensively performed for various drift-wave-type instabilities, to identify characteristics of dominant turbulent fluctuation in various parameter regimes. The other piece of the classic paradigm, decorrelation by nonlinear mode-mode interactions, has been studied via renormalization program within the framework of direct-interaction approximation. Details of the renormalization process is presented in section 2.1.

Experimental finding of H-mode, the most promising enhanced tokamak operation mode to date characterized by steep profile gradients in edge pedestal region, stimulated extensive theoretical studies on physical machanisms of transport barrier formation accompanied by turbulence suppression. Both experimentally and theoretically, roles of mean E×B flow have been recognized to be crucial for transport barrier formation. Especially, enhancement of turbulence decorrelation by radial shear of mean E×B flow has been widely accepted as a universal mechanism for turbulence suppression and transport barrier formation toward an enhanced confinement regime in toroidal fusion devices. In addressing theories of the E×B flow shear induced enhancement of decorrelation of tokamak turbulence, two-point renormalization program and two-point decorrelation theory, first developed by T.H. Dupree in 1D Vlasov system since ‘70s, has been applied to tokamak plasma turbulence in earnest from late ‘80s.

Note that one-point theories contain effects of mean E×B shear flows on linear growth rate or nonlinear decorrelation rate of turbulence via modification of the linear propagator, but what's more universal and important is enhancement of the decorrelation as a consequence of hybridization of the decorrelation process by E×B flow shear. This can only be captured in a two-point equation. Details of the E×B shear induced enhancement of turbulence decorrelation is presented in section 2.5.

While two-point theories focus on details of turbulence suppression by E×B shearing, generation of mean E×B shear flows from turbulence has been suggested since early '90s in a theoretical point of view. The turbulence-generated E×B flows are called zonal flows. Note that the zonal flow generation is equivalent to the suppression of turbulence by zonal flow shear, that is, turbulence and zonal flows directly interact with each other. The interaction between tokamak turbulence and zonal flows has been theoretically interpreted using predator–prey type models, which reveal bifurcation property of turbulence state and limit-cycle oscillation (LCO). LCO is a signature of the turbulence-zonal flow interaction, which consist of alternating quasi-periodic oscillations of populations of predator (zonal flows) and prey (turbulence). After several periods of the oscillations, zonal flows can lead tokamak turbulence to a bifurcated state with reduced amplitude. An important factor in the bifurcation is damping of zonal flows, because zonal flow generation rate should exceed the damping rate for a bifurcation. Zonal flow damping in tokamak plasmas has been theoretically studied following pioneering works of M.N. Rosenbluth and F.L. Hinton in late '90s, in which finite residual zonal flow level after fast collisionless decay was identified by a gyrokinetic study and long-term collisional damping of residual zonal flows was analyzed using a drift-kinetic equation.

Nowadays, researchers in magnetic fusion energy community often divide mean E×B flows into two classes. One is macroscale (in both spatial and temporal scales) E×B flows that satisfy radial force balance, a constraint for profiles coming from radial component of ion momentum equation, and the other one is mesoscale zonal flows which are generated from turbulence via Reynolds stress and directly interact with turbulence. Note that since radial dynamics of zonal flows is important in many cases, radial force balance should not be applied in estimating zonal flow level in a strict sense. It is widely believed that zonal flows play a key role in triggering transition to an enhanced confinement regime, but whether to focus on physics of E×B shearing or that of zonal flow–turbulence interaction to determine a proper transition criterion is still open to dispute.

Dispite deepened understanding of roles of E×B shear flows on turbulence suppression, there still remain issues on transport barrier formation which cannot be explained by classic theories but are practically important for an efficient high-performance tokamak operation. I am especially interested in 1. up-down asymmetry of H-mode transition power threshold in single-null diverted plasmas, 2. different behavior of electron thermal internal transport barrier (ITB) formation from those of ion thermal and density ITBs, and 3. increase of H-mode transition power threshold in the presence of resonant magnetic perturbations (RMPs). These three issues are discussed in this thesis with my newly extended theories of E×B shear suppression and zonal flow evolution.

Remaining part of this thesis is organized as follows. In chapter 2, I describe how the shape of an initially tilted turbulence eddy is represented in a two-point theory, after a brief introduction to renormalization of tokamak turbulence and ballooning mode formalism. Through a moment analysis of a two-point equation, I analyze E×B flow shear induced distortion of an initially tilted eddy

in detail, and identify sign-dependence of E×B flow shear induced turbulence suppression. I discuss an application of the result to the issue of up-down asymmetry of H-mode transition threshold in single-null diverted plasmas. In chapter 3, I systematically derive a proper two-point equation for trapped electron turbulence, starting from modern bounce-kinetic formalism. A new criterion for suppression of trapped electron turbulence is suggested via a moment analysis, and synergism between E×B flow shear and trapped electron precession shear is identified. Relevance of my theory to experimental observations of electron thermal internal transport barrier formation is discussed. Finally, in chapter 4, I present an analytical study of zonal flow evolution in a tokamak plasma in the presence of externally imposed RMPs, using gyrokinetic equations. RMP-induced long-time collisionless decay of residual zonal flows is identified, and its parameter (e.g., ion temperature or toroidal mode number of RMP) dependence and impact on H-mode transition threshold are discussed.

Chapter 2

E×B shear suppression of tilted eddies

In magnetic fusion energy research community, it is widely accepted that E×B flow shear can significantly reduce tokamak plasma turbulence, therefore forming local transport barrier [1–5]. Two point nonlinear decorrelation theory, first developed in 1D Vlasov system [6], has been applied to tokamak plasmas to describe non-wave-like eddy structures in plasma turbulence [7–9]. Ref. [8] addresses how the E×B flow shear can reduce the radial correlation length of a turbulence eddy in a magnetized plasma. The original calculation in cylindrical geometry [8] has been extended to more realistic equilibrium magnetic field configurations over the years [10–12]. These calculations specify the initial size of an eddy in radial and binormal directions. But the eddies are assumed to be perfectly aligned radially in the absence of the E×B shear flow. In toroidal geometry, poloidal asymmetry and shear of the magnetic field can make turbulence eddy tilted with a finite angle with respect to the radial direction.

In this chapter, I present a theoretical study of the effect of initial tilting of turbulence eddies on the effectiveness of E×B shear induced turbulence suppression in tokamak geometry. Specifically, I extend the work of Ref. [11] by including this effect. Here, initial tilting refers to tilting of an eddy from the radial direction due to origins other than E×B flow shear. First of all, I introduce the conecpt of renormalization for tokamak turbulence, necessary to understand theories of E×B shear suppression. I step forward to renormalization of a two-point equation which describes evolution of two-point correlation function. Clear difference between one-point and two-point renormalizations is emphasized, and non-wave-like turbulence eddies are introduced as an important class of constituents of turbulence. After a short explanation of ballooning mode formalism, I perform a theoretical analysis of E×B flow shear effect on tilted eddies. The principal results are as follows.

1. The E×B shear effects can be characterized as a combination of the eddy size reduction along the principal axis and the rotation of the eddy, and consequent change in the eddy size projected on the radial direction.

2. For typical situations with a small initial eddy tilting, an initial tilting in the same direction as the E×B flow shear makes the E×B shear reduction of turbulence more efficient compared to the no-initial-tilting case, while an initial tilting in the opposite direction with respect to the E×B shear makes the shearing less efficient.

3. This dependence on relative sign is more pronounced as the eddy is more elongated in the radial direction compared to the binormal direction and as the initial angle of tilting with respect to the radial direction gets larger.

2.1 Renormalization for tokamak turbulence

An equation describing time evolution of turbulent fluctuations of a continuum field h in magnetized plasmas can be written as follows.

$$\left(g_0^{-1} + \delta\mathbf{v}_{\mathrm{E}} \cdot \boldsymbol{\nabla}\right) \delta h = -\delta\mathbf{v}_{\mathrm{E}} \cdot \boldsymbol{\nabla} h_0. \tag{2.1}$$

Here, $h = h_0 + \delta h$, where h_0 is the mean part and δh is the fluctuating part. A continuum field h can be a distribution function f for a kinetic description, or a velocity moment such as a density n or a pressure p for a fluid description. g_0^{-1} is an inverse linear propagator of δh, e.g., $\partial_t + v_\parallel \nabla_\parallel + \mathbf{v}_{\mathrm{d}} \cdot \boldsymbol{\nabla}$ for a gyrokinetic Vlasov equation, where $v_\parallel$ and $\mathbf{v}_{\mathrm{d}}$ are parallel streaming and mean drift velocities, respectively. $\delta\mathbf{v}_{\mathrm{E}} = \mathbf{b} \times \boldsymbol{\nabla}\delta\phi/B$ is fluctuating E×B drift velocity, where $B = |\mathbf{B}|$ is magnetic field strength, $\mathbf{b} = \mathbf{B}/B$ is a unit vector in the magnetic field direction and $\delta\phi$ is fluctuating electrostatic potential. Note that I keep E×B nonlinearity only as a sole representative one among various nonlinearities which appear describing turbulence in magnetized plasmas. Indeed, it has been demonstrated that E×B nonlinearity has a dominant influence in tokamak turbulence [13–18]. The nonlinearity is full of numerous nonlinear couplings which are too diverse to understand at once. Thus, to identify and understand specific important nonlinear properties from the nonlinearity, we have to perform a systematic approximation of the nonlinearity, namely, renormalization.

The necessity of a renormalization become more transparent when we consider the Fourier decomposed version of Eq. (2.1),

$$g_{0,\mathbf{k},\omega}^{-1} h_{\mathbf{k},\omega} + \mathcal{N}_{\mathbf{k},\omega} = -\mathbf{v}_{\mathrm{E},\mathbf{k},\omega} \cdot \boldsymbol{\nabla} h_0, \tag{2.2}$$

where the E×B nonlinearity $N_{\mathbf{k},\omega}$ is

$$\mathcal{N}_{\mathbf{k},\omega} = \sum_{\substack{\mathbf{k}=\mathbf{k}'+\mathbf{k}'' \\ \omega=\omega'+\omega''}} \mathbf{v}_{\mathrm{E},\mathbf{k}',\omega'} \cdot i\mathbf{k}'' h_{\mathbf{k}'',\omega''}. \tag{2.3}$$

Hereafter I drop the symbol "δ" in front of a Fourier-decomposed fluctuating quantity for our convenience. What we want is an equation, each term of which is proportional to $h_{\mathbf{k},\omega}$ or $\phi_{\mathbf{k},\omega}$. To obtain it, we should look into an equation for $h_{\mathbf{k}'',\omega''}$,

$$g^{-1}_{0,\mathbf{k}'',\omega''} h_{\mathbf{k}'',\omega''} + \mathcal{N}_{\mathbf{k}'',\omega''} = -\mathbf{v}_{\mathrm{E},\mathbf{k}'',\omega''} \cdot \boldsymbol{\nabla} h_0, \tag{2.4}$$

where

$$\mathcal{N}_{\mathbf{k}'',\omega''} = \sum_{\substack{\mathbf{k}''=\mathbf{k}'''+\mathbf{k}'''' \\ \omega''=\omega'''+\omega''''}} \mathbf{v}_{\mathrm{E},\mathbf{k}''',\omega'''} \cdot i\mathbf{k}'''' h_{\mathbf{k}'''',\omega''''}. \tag{2.5}$$

Note that we cannot obtain a relation between $h_{\mathbf{k}'',\omega''}$ and $h_{\mathbf{k},\omega}$, $\phi_{\mathbf{k},\omega}$ from this equation. Instead, we now have one more task of relating $h_{\mathbf{k}'''',\omega''''}$ to $h_{\mathbf{k}'',\omega''}$, $\phi_{\mathbf{k}'',\omega''}$ or $h_{\mathbf{k},\omega}$, $\phi_{\mathbf{k},\omega}$. Similarly, looking into an equation for $h_{\mathbf{k}'''',\omega''''}$ brings an additional task to us. we should close such a hierarchy with a proper approximation, i.e., we need a renormalization. Be aware, however, that the motivation introduced above is appropriate only for the situations where modal expansion of fluctuations works well.

The purpose of the renormalization is to approximate the nonlinearity by a form $\mathcal{N}_{\mathbf{k},\omega} = d_{\mathbf{k},\omega} h_{\mathbf{k},\omega} - \beta_{\mathbf{k},\omega}\phi_{\mathbf{k},\omega}$, where $d_{\mathbf{k},\omega}$ and $\beta_{\mathbf{k},\omega}$ are operators that may depend on Fourier components of δh and $\delta\phi$. For this, I assume that the mode $(\mathbf{k}'', \omega'')$ in Eq. (2.3) is driven only by direct beating of $(\mathbf{k}, \omega)$ and $(\mathbf{k}', \omega')$. That is, we consider only one triad coupling for given $\mathbf{k}$ and $\mathbf{k}'$. Then, Eq. (2.4) is approximated by

$$h_{\mathbf{k}'',\omega''} = -g_{\mathbf{k}-\mathbf{k}',\omega-\omega'} \left\{ \mathbf{v}_{\mathrm{E},\mathbf{k},\omega} \cdot (-i\mathbf{k}') h_{-\mathbf{k}',-\omega'} + \mathbf{v}_{\mathrm{E},-\mathbf{k}',-\omega'} \cdot i\mathbf{k} h_{\mathbf{k},\omega} \right\}, \tag{2.6}$$

where $g_{\mathbf{k},\omega}$ is the renormalized propagator of which definition is given by $g^{-1}_{\mathbf{k},\omega} = g^{-1}_{0,\mathbf{k},\omega} + d_{\mathbf{k},\omega}$. Substituting Eq. (2.6) into Eq. (2.3) and changing dummy variables, the renormalized nonlinearity is obtained as follows [19].

$$\mathcal{N}_{\mathbf{k},\omega} = d_{\mathbf{k},\omega} h_{\mathbf{k},\omega} - \beta_{\mathbf{k},\omega}\phi_{\mathbf{k},\omega}, \tag{2.7}$$

where

$$d_{\mathbf{k},\omega} = \frac{1}{B^2}\sum_{\mathbf{k}',\omega'} (\mathbf{k}\cdot\mathbf{k}'\times\mathbf{b})^2 g_{\mathbf{k}+\mathbf{k}',\omega+\omega'} |\phi_{\mathbf{k}',\omega'}|^2, \tag{2.8}$$

and

$$\beta_{\mathbf{k},\omega} = \frac{1}{B^2}\sum_{\mathbf{k}',\omega'} (\mathbf{k}\cdot\mathbf{k}'\times\mathbf{b})^2 g_{\mathbf{k}+\mathbf{k}',\omega+\omega'} \phi_{-\mathbf{k}',-\omega'} h_{\mathbf{k}',\omega'}. \tag{2.9}$$

Therefore, the renormalized equation for $h_{\mathbf{k},\omega}$ is,

$$(g^{-1}_{0,\mathbf{k},\omega} + d_{\mathbf{k},\omega}) h_{\mathbf{k},\omega} = -\mathbf{v}_{\mathrm{E},\mathbf{k},\omega}\cdot\boldsymbol{\nabla} h_0 + \beta_{\mathbf{k},\omega}\phi_{\mathbf{k},\omega}. \tag{2.10}$$

Here $d_{\mathbf{k},\omega}$ represents scattering of the trajectory of a test 'particle' $h_{\mathbf{k},\omega}$ due to ambient 'fields' $\phi_{\mathbf{k}',\omega'}$s. Combining $d_{\mathbf{k},\omega}$ with $-i\omega$ from $g^{-1}_{0,\mathbf{k},\omega}$, it becomes clear that the nonlinear scattering induces decorrelation of the fluctuating field $h_{\mathbf{k},\omega}$. The second term on the right-hand side (RHS) of Eq. (2.10), which is proportional to $\beta_{\mathbf{k},\omega}$, represents nonlinear modification of turbulence source. Recall that the first term on RHS corresponds to the linear driving source of turbulence. Note that the second term is necessary for a conservative formulation that does not produce any unphysical perpendicular heating [19].

In a hydrodynamic limit, $|\mathbf{k}| \ll |\mathbf{k}'|$ and $|\omega| \ll |\omega'|$, and thus the expression of the nonlinear scattering term $d_{\mathbf{k},\omega}$ is approximated by [19]

$$d_{\mathbf{k},\omega} \simeq \frac{1}{B^2}\sum_{\mathbf{k}',\omega'} (\mathbf{k}\cdot\mathbf{k}'\times\mathbf{b})^2 \frac{|\phi_{\mathbf{k}',\omega'}|^2}{g^{-1}_{0,\mathbf{k}',\omega'} + d_{\mathbf{k}',\omega'}} \equiv \mathbb{D} : \mathbf{k}_\perp\mathbf{k}_\perp. \tag{2.11}$$

The physical meaning of Eq. (2.11) becomes more transparent when we employ resonance broadening theory [20, 21]. Consider a formal solution of an equation

for $h_{\mathbf{k},\omega}$, which should be identical with Eq. (2.1), is [22]

$$\begin{aligned} h_{\mathbf{k},\omega} &= e^{-i\mathbf{k}\cdot\mathbf{x}} \int_0^\infty d\tau\, e^{i\omega\tau} \langle u(-\tau)\rangle_{\mathrm{O}} e^{i\mathbf{k}\cdot\mathbf{x}} S_{\mathbf{k},\omega} \\ &= \int_0^\infty d\tau\, e^{i[\omega\tau + \mathbf{k}\cdot\{\mathbf{x}_0(-\tau)-\mathbf{x}_0(0)\}]} \langle e^{i\mathbf{k}\cdot\delta\mathbf{x}_\perp(-\tau)}\rangle_{\mathrm{O}} S_{\mathbf{k},\omega}, \end{aligned} \tag{2.12}$$

where $u(-\tau)$ is an orbit propagator that satisfies $u(-\tau)e^{i\mathbf{k}\cdot\mathbf{x}} = e^{i\mathbf{k}\cdot\mathbf{x}(-\tau)}$, i.e. it relates a position $\mathbf{x}$ and a trajectory $\mathbf{x}(t)$. The bracket $\langle\cdots\rangle_{\mathrm{O}}$ is an average over an ensemble of orbits. $S_{\mathbf{k},\omega}$ represents source of random fluctuations. Note that we decomposed the total trajectory $\mathbf{x}_\perp(t) = \mathbf{x}_{\perp 0}(t) + \delta\mathbf{x}_\perp(t)$, where $\delta\mathbf{x}_\perp$ is excursion in perpendicular position by random E×B scattering. Initial time $t = 0$ is set to be $\mathbf{x}_{\perp 0}(0) = \mathbf{x}$. Assuming that probability of $\delta\mathbf{x}_\perp$ have a Gaussian distribution,

$$\langle e^{i\mathbf{k}\cdot\delta\mathbf{x}_\perp(-\tau)}\rangle_{\mathrm{O}} = \langle 1 + i\mathbf{k}_\perp\cdot\delta\mathbf{x} - (\mathbf{k}_\perp\cdot\delta\mathbf{x}_\perp)^2/2 + \cdots\rangle_{\mathrm{O}} = e^{-(\mathbb{D}_{\mathrm{RBT}}:\mathbf{k}_\perp\mathbf{k}_\perp)\tau}, \tag{2.13}$$

where $\mathbb{D}_{\mathrm{RBT}}\tau$ corresponds to the inverse width of the Gaussian distribution of $\delta\mathbf{x}_\perp$. Then, we obtain a form of renormalized response

$$h_{\mathbf{k},\omega} = \int_0^\infty d\tau\, e^{i[(\omega + i\mathbb{D}_{\mathrm{RBT}}:\mathbf{k}_\perp\mathbf{k}_\perp)\tau + \mathbf{k}\cdot\{\mathbf{x}_0(-\tau)-\mathbf{x}_0(0)\}]} S_{\mathbf{k},\omega}. \tag{2.14}$$

Nonlinear modification of frequency $-i\omega \to -i\omega + \mathbb{D}_{\mathrm{RBT}} : \mathbf{k}_\perp\mathbf{k}_\perp$ in resonance broadening theory has the same form with that in a conservative renormalization formulation. Note that effect of the modification can be interpreted as $\gamma_{\mathrm{eff},\mathbf{k}} = \gamma_{\mathrm{lin},\mathbf{k}} - \Delta\omega_{\mathbf{k}}$, where $\gamma_{\mathrm{lin},\mathbf{k}}$ is the linear growth rate and $\Delta\omega_{\mathbf{k}} = \mathbb{D} : \mathbf{k}_\perp\mathbf{k}_\perp$ is the nonlinear decorrelation rate. This relation is often used for a rough estimation of radial turbulent diffusivity D in the presence of nonlinearly saturated turbulence, taking $\gamma_{\mathrm{eff},\mathbf{k}} = 0$ for a representative $\mathbf{k}$ with $\Delta\omega_{\mathbf{k}} \sim Dk_\perp^2$. Now, it is evident that Eq. (2.11) represents nonlinear decorrelation due to diffusive (recall $i\mathbf{k} \leftrightarrow \boldsymbol{\nabla}$) scattering of a continuum element by ambient Gaussian fluctuations.

I close this section with the configuration space version of the renormalized equation in hydrodynamic limit.

$$\left(g_0^{-1} - \mathbb{D} : \boldsymbol{\nabla}\boldsymbol{\nabla}\right) \delta h = S. \tag{2.15}$$

Here S is the renormalized turbulence source.

2.2 Two-point renormalization

In the previous section, I presented a standard renormalization process for an equation of fluctuating continuum field $\delta h(\mathbf{x}, t)$. However, it is often more relevant considering two-point correlations of fluctuating fields to study physical properties of turbulent structures. In this section, I present a renormalization process for a two-point correlation $\langle \delta h(1) \delta h(2) \rangle$, where the indices (1) and (2) denote position (in configuration space or phase space) and time of continuum elements 1 and 2, respectively. $\langle \cdots \rangle$ is an ensemble average. Then, from Eq. (2.1), after a symmetrization, one obtain the following form of two-point equation.

$$g_0^{-1}(1,2) \langle \delta h(1) \delta h(2) \rangle + T(1,2) = P(1,2), \tag{2.16}$$

where the expression of the E×B mixing term $T(1,2)$ is

$$T(1,2) = \langle \delta \mathbf{v}_{\mathrm{E}}(1) \cdot \boldsymbol{\nabla}_1 (\delta h(1) \delta h(2)) \rangle + (1 \leftrightarrow 2). \tag{2.17}$$

Here $(1 \leftrightarrow 2)$ denotes a permutation of variables 1 and 2. $g_0(1,2)$ is the two-point propagator that contains the time evolution term ∂_t and mean convection terms. $P(1,2)$ represents production of the two-point correlation by a gradient of the mean continuum field h_0. For a renormalization, we Fourier-transform the first term on RHS of Eq. (2.17) to

$$\sum_{\substack{\mathbf{k},\mathbf{k}',\mathbf{k}'' \\ \omega,\omega',\omega''}} \left\langle e^{i(\omega+\omega'+\omega'')t} e^{i(\mathbf{k}+\mathbf{k}')\cdot\mathbf{x}_1} e^{i\mathbf{k}''\cdot\mathbf{x}_2} \mathbf{v}_{\mathrm{E},\mathbf{k},\omega} \cdot i\mathbf{k}' h_{\mathbf{k}',\omega'} h_{\mathbf{k}'',\omega''} \right\rangle, \tag{2.18}$$

and similarly for the second term. We introduce average and relative variables $\mathbf{x}_+ = (\mathbf{x}_1 + \mathbf{x}_2)/2$ and $\mathbf{x}_- = \mathbf{x}_1 - \mathbf{x}_2$, respectively. Then, We approximate the ensemble average by average over long time and spatial periods of fluctuation pattern [23]. For simplicity, we assume that the approximation is well-satisfied for each spatial direction x_+^i $(i = 1, 2, 3)$. Then, Eq. (2.18) is approximated by

$$\sum_{\substack{\mathbf{k},\mathbf{k}' \\ \omega,\omega'}} e^{(\mathbf{k}+\mathbf{k}')\cdot\mathbf{x}_-} \mathbf{v}_{\mathrm{E},\mathbf{k},\omega} \cdot i\mathbf{k}' h_{\mathbf{k}',\omega'} h_{-\mathbf{k}-\mathbf{k}',-\omega-\omega'}$$
$$- \sum_{\substack{\mathbf{k},\mathbf{k}'' \\ \omega,\omega''}} e^{-i\mathbf{k}''\cdot\mathbf{x}_-} \mathbf{v}_{\mathrm{E},\mathbf{k},\omega} \cdot i(\mathbf{k}+\mathbf{k}'') h_{-\mathbf{k}''-\mathbf{k},-\omega''-\omega} h_{\mathbf{k}'',\omega''}. \tag{2.19}$$

We properly change dummy variables, and assume that an induced mode is driven only by direct beating of other two modes of a triad of nonlinear coupling, just as in section 2.1. Then, in hydrodynamic limit, Eq. (2.19) becomes

$$-\sum_{\mathbf{k},\omega} \Big(\sum_{\mathbf{k}',\omega'} g_{\mathbf{k}',\omega'} \mathbf{v}_{\mathrm{E},\mathbf{k}',\omega'} \mathbf{v}_{\mathrm{E},-\mathbf{k}',-\omega'} \Big) : i\mathbf{k} i\mathbf{k} e^{i\mathbf{k}\cdot\mathbf{x}_-} |h_{\mathbf{k},\omega}|^2$$
$$-\sum_{\mathbf{k},\omega} \Big(\sum_{\mathbf{k}',\omega'} e^{i\mathbf{k}'\cdot\mathbf{x}_-} g_{\mathbf{k}',\omega'} \mathbf{v}_{\mathrm{E},\mathbf{k}',\omega'} \mathbf{v}_{\mathrm{E},-\mathbf{k}',-\omega'} \Big) : i\mathbf{k}(-i\mathbf{k}) e^{i\mathbf{k}\cdot\mathbf{x}_-} |h_{\mathbf{k},\omega}|^2. \tag{2.20}$$

I do not present terms related to mixed correlations between $\delta\phi$ and δh, which are naturally obtained by this two-point renormalization but are not of my main interest. As expalined in section 2.1, they correspond to nonlinear modifications of the production term. Note that the Fourier-transformed expression of the two-point correlation is

$$\langle \delta h(1) \delta h(2) \rangle = \sum_{\mathbf{k},\omega} e^{i\mathbf{k}\cdot\mathbf{x}_-} |h_{\mathbf{k},\omega}|^2. \tag{2.21}$$

Therefore, repeating the same process for the second term on RHS of Eq. (2.17) and going back to the real space, we obtain a renormalized expression of the

mixing term as follows.

$$T(1,2) \simeq -(\mathbb{D}_{11} : \boldsymbol{\nabla}_1\boldsymbol{\nabla}_1 + \mathbb{D}_{21} : \boldsymbol{\nabla}_2\boldsymbol{\nabla}_1 + \mathbb{D}_{12} : \boldsymbol{\nabla}_1\boldsymbol{\nabla}_2 + \mathbb{D}_{22} : \boldsymbol{\nabla}_2\boldsymbol{\nabla}_2)\langle \delta h(1)\delta h(2)\rangle, \tag{2.22}$$

where

$$\mathbb{D}_{11} = \mathbb{D}_{22} = \sum_{\mathbf{k}',\omega'} g_{\mathbf{k}',\omega'}\mathbf{v}_{\mathrm{E},\mathbf{k}',\omega'}\mathbf{v}_{\mathrm{E},-\mathbf{k}',-\omega'}, \tag{2.23}$$

$$\mathbb{D}_{21} = \mathbb{D}_{12} = \sum_{\mathbf{k}',\omega'} e^{i\mathbf{k}'\cdot\mathbf{x}_-} g_{\mathbf{k}',\omega'}\mathbf{v}_{\mathrm{E},\mathbf{k}',\omega'}\mathbf{v}_{\mathrm{E},-\mathbf{k}',-\omega'}. \tag{2.24}$$

Note that Eq. (2.22) are symmetric on a permutation $1 \leftrightarrow 2$. Here, $\mathbb{D}_{11}$ and $\mathbb{D}_{22}$ represent independent turbulent diffusion of continuum elements, that already exist in Eq. (2.15), the renormalized one-point equation. Meanwhile, the cross-diffusion terms with $\mathbb{D}_{21}$ and $\mathbb{D}_{12}$ are new ones which are absent in the one-point equation. Their role becomes more transparent with a description of Eq. (2.22) using average and relative coordinates. Considering implicit ensemble average which has been approximated by spatial average over average coordinates,

$$T(1,2) \simeq -\mathbb{D}_{\mathrm{rel}} : \boldsymbol{\nabla}_-\boldsymbol{\nabla}_-, \tag{2.25}$$

where

$$\begin{aligned}\mathbb{D}_{\mathrm{rel}} &= \mathbb{D}_{11} + \mathbb{D}_{22} - \mathbb{D}_{21} - \mathbb{D}_{12} \\ &= \sum_{\mathbf{k}',\omega'} (1 - \cos(\mathbf{k}\cdot\mathbf{x}_-)) g_{\mathbf{k}',\omega'}\mathbf{v}_{\mathrm{E},\mathbf{k}',\omega'}\mathbf{v}_{\mathrm{E},-\mathbf{k}',-\omega'}\end{aligned} \tag{2.26}$$

is the relative diffusion matrix. Note that for a large separation $k^2x_-^2 > 1$, the relative diffusion becomes $\mathbb{D}_{\mathrm{rel}} \simeq \mathbb{D}_{11} + \mathbb{D}_{22}$, so that it asymptotes to that of two independent elements. For a small separation $k^2x_-^2 < 1$, each component of $\mathbb{D}_{\mathrm{rel}}$ becomes proportional to $k^2x_-^2$, so that the relative diffusion asymptotes to zero in the limit $1 \to 2$. Now, it is clear that $\mathbb{D}_{21}$ and $\mathbb{D}_{12}$ make trajectories

of two neighboring elements 1 and 2 to be correlated with each other, so that the elements tend to move together.

As a consequence, a new class of participant, turbulence eddies, enters to the turbulent bath, in addition to waves [23]. Waves are fluctuations that follow an one-point equation Meanwhile, turbulence eddies refer to non-wave-like fluctuating structures consisting of continuum elements having correlated tarjectories, which are described by a two-point equation. That is, turbulence eddies are long-lived turbulent structures (than waves) that behave like macroparticles. Note that a fluctuating continuum field δh is decomposed by $\delta h = h^c + \tilde{h}$, where h^c and $\tilde{h}$ are called coherent and incohernet fluctuation, respectively. The coherent piece h^c is wave-like, i.e., it follows a renormalized one-point equation, and the incoherent piece $\tilde{h}$, which represents small-scale granulations, induces trajectory correlation. A turbulence eddy consists of contributions from both coherent and incoherent pieces, and its non-wave-like character originates from the incoherent piece. In the later part of chapter 2 and in chapter 3, I present theoretical studies on effect of fundamental mean convections to a turbulence eddy, using renormalized two-point equations that I introduced in this section.

2.3 Ballooning mode formalism

The ballooning mode formalism is a theoretical framework developed for an appropriate treatment of high toroidal mode number perturbations of a toroidal magnetized plasma. A cylindrical plasma is properly described with cylindrical coordinates (r, θ, ϕ), where r is the radial position, and θ and ϕ are the poloidal and the toroidal angles, respectively. Perturbations in a cylindrical plasma are studied by analyzing a Fourier-decomposed mode which is identified by indices (m, n). Here, m and n are the poloidal and the toroidal mode numbers, respec-

tively. However, this way of decomposition is not appropriate to study tokamak turbulence because the poloidal mode number m is no longer a good quantum number due to poloidal angle dependence of tokamak magnetic field; different m-harmonics can couple with each other even in linear theory. Ballooning mode formalism provides an appropriate decomposition of perturbations relevant to plasmas in a tokamak magnetic field. The formalism also applies to high-n MHD instabilities as well as microturbulence.

In this section, I shortly explain the ballooning transformation following Ref. [24]. Consider an axisymmetric magnetic field that can be expressed as

$$\mathbf{B} = \boldsymbol{\nabla}\psi \times \boldsymbol{\nabla}\zeta + I(\psi)\boldsymbol{\nabla}\zeta, \tag{2.27}$$

where ψ is the toroidal magnetic flux that play a role of magnetic surface label and ζ is the toroidal angle. We then introduce orthogonal coordinates (ψ, ζ, χ) where χ is the poloidal angle. The metric for these coordinates is

$$ds^2 = (d\psi/RB_\chi)^2 + (JB_\chi d\chi)^2 + (Rd\zeta)^2, \tag{2.28}$$

and the volume element is $d\tau = Jd\psi d\chi d\zeta$, where J is the Jacobian. Here, R is the major radius, i.e. the distance from the magnetic axis. A magnetic field line is defined by $\psi = \text{const}$ and $\chi = \chi_0(\zeta)$. We then define $\nu \equiv d\zeta/d\chi_0 = IJ/R^2$ as the local safety factor, a measure of pitch angle of a magnetic field line. The safety factor q is defined as $q = \oint \nu d\chi/2\pi$.

The usual representation of a short-wavelength perturbation ϕ in a slowly-varying medium is an eikonal representation $\phi \propto F\exp(inS)$, where the phase nS varies rapidly ($n \gg 1$), but F and S vary slowly. In our system, strong magnetic field brings a strong anisotropy, so that turbulent fluctuations have short wavelength perpendicular to the magnetic field ($n\boldsymbol{\nabla}_\perp S \sim \mathcal{O}(1)$) but long wavelength parallel to it ($n\mathbf{b}\cdot\boldsymbol{\nabla}S = 0$). Since ζ is an ignorable coordinate, a

possible eikonal expression for fluctuations containing the isotropy is

$$\phi = F(\psi, \chi) \exp\left[in\left(\zeta - \int_{\chi_0}^{\chi} \nu d\chi\right)\right]. \tag{2.29}$$

In this expression, parallel variation of the fluctuation and effect of the slowly-varying medium are both included in the slowly-varying function $F(\psi, \chi)$. One may consider Eq. (2.29) as an appropriate representation for a turbulent fluctuation in a tokamak plasma. However, since a tokamak magnetic field is radially sheared, $\nu(\psi)$ varies radially and thus it is impossible to reconcile it with the periodicity constraint, $\phi(\chi) = \phi(\chi + 2\pi p)$ for an arbitrary integer p, without giving up the whole concept of an eikonal representation. Note that $n \oint \nu d\chi/2\pi$ is not an integer in general. Therefore, we need an alternative representation for a perterbation in a tokamak plasma.

After a Fourier decomposition in the toroidal angle ζ, an ignorable coordinate, a linear analysis of perturbations in an axisymmetric magnetic field can be reduced to a 2D eigenvalue problem

$$\mathcal{L}(\chi, \psi)\phi_n(\chi, \psi) = \lambda\phi_n(\chi, \psi). \tag{2.30}$$

Here, the linear operator $\mathcal{L}$ is periodic in χ, where $0 \leq \chi < 2\pi$, and ϕ must be periodic in χ and bounded in ψ. We now introduce the ballooning transformation of ϕ_n,

$$\phi_n(\chi, \psi) = \sum_m e^{-im\chi} \int_{-\infty}^{\infty} e^{im\eta} \hat{\phi}_n(\eta, \psi) d\eta, \tag{2.31}$$

which automatically ensures periodicity of ϕ_n in χ. Note that the ballooning-transformed function $\hat{\phi}_n$ do not need to be periodic in η. Substituting Eq. (2.31) into Eq. (2.30), it is obvious that $\hat{\phi}_n(\eta, \psi)$, which is a solution of

$$\mathcal{L}(\eta, \psi)\hat{\phi}_n(\eta, \psi) = \lambda\hat{\phi}_n(\eta, \psi) \tag{2.32}$$

in the infinite domain of the ballooning angle $-\infty < \eta < \infty$, generate a solution $\phi(\chi, \psi)$ of Eq. (2.30) that is periodic in χ, with the same eigenvalue. Now,

the ballooning-transformed function $\hat{\phi}_n(\eta, \psi)$ is successfully represented in an eikonal form

$$\hat{\phi}_n(\eta, \psi) \exp(in\zeta) = F(\eta, \psi) \exp\left[in\left(\zeta - \int_{\eta_0}^{\eta} \nu(\eta, \psi) d\eta\right)\right], \tag{2.33}$$

without any issue on periodicity. $\hat{\phi}_n$ in this form is called a quasi-mode. The slowly-varying amplitude $F(\eta, \psi)$ can be calculated as an expansion in n^{-1}. In the lowest order, the quasi-mode satisfies an ordinary differential equation in the ballooning angle η. Note that fast radial variation (i.e. variation in ψ) of the quasi-mode is characterized by an equivalent wavenumber $k_\psi = -n \int_{\eta_0}^{\eta} d\eta \partial\nu/\partial\psi$ in the lowest-order equation. Slower radial variation, which corresponds to the variation of F in ψ, is captured in higher-order equations. To complete the eigenvalue problem in the ballooning space, we need proper boundary conditions in η. As $|\eta| \to \infty$, $\hat{\phi}_n$ must behave such that the integration in Eq. (2.31) converges, and in many cases this is a sufficient condition for distinguishing acceptable solutions from non-acceptable ones.

An alternative representation of the structure of the solution $\phi_n(\chi, \psi)$ generated by $\hat{\phi}_n(\eta, \psi)$ is as follows. Assuming proper convergence properties,

$$\phi_n(\chi, \psi) = \int_{-\infty}^{\infty} \sum_m e^{-im(\chi - \eta)} \hat{\phi}_n(\eta, \psi) d\eta. \tag{2.34}$$

Then, we can regard the summation over m as

$$\sum_m e^{-im(\chi - \eta)} = \sum_N \delta(\chi - \eta - 2\pi N), \tag{2.35}$$

where N is an integer, and thus rewrite Eq. (2.34) as

$$\phi_n(\chi, \psi) = \sum_N \hat{\phi}_n(\chi - 2\pi N, \psi). \tag{2.36}$$

Recalling that $\hat{\phi}_n$ is a quasi-mode, we again see that ϕ_n is an infinite sum of quasi-modes.

2.4 Description of an initially tilted turbulence eddy

Now, we proceed to my work on E×B shear induced suppression of an initially tilted tokamak turbulence eddy. As in previous works [8,10,11], a one-field fluid model is adopted, in which a fluctuating field δH is convected by a mean E×B shear flow $\mathbf{u}_E$ and a fluctuating E×B flow $\tilde{\mathbf{u}}_E$,

$$(\partial/\partial t + \mathbf{u}_E \cdot \boldsymbol{\nabla} + \tilde{\mathbf{u}}_E \cdot \boldsymbol{\nabla})\, \delta H = S, \tag{2.37}$$

where $\mathbf{u}_E = \mathbf{B} \times \boldsymbol{\nabla}\Phi_0/B^2$, $\tilde{\mathbf{u}}_E = \mathbf{B} \times \boldsymbol{\nabla}\delta\Phi/B^2$, and S is the driving source of the turbulence. Linear dissipation and subdominant nonlinearities other than E×B nonlinearity are ignored for simplicity. We use the ballooning representation in magnetic coordinates for a natural representation of the small scale (high mode number) fluctuating field in tokamaks. The mean electrostatic potential Φ_0 is assumed to be a flux function, i.e. $\Phi = \Phi(\psi)$. The expression of the E×B nonlinearity using the ballooning mode formalism is given by Ref. [25]. Two-point equation is then derived following standard procedure [6] of symmetrization with respect to (ψ_1, ϕ_1, η_1) and (ψ_2, ϕ_2, η_2), applying average and relative coordinates, followed by an ensemble average. Through a two-point renormalization with a Gaussian spectrum of the electrostatic potential [7], we successfully approximate the E×B nonlinearity to the relative turbulent diffusion in the binormal direction as follows.

$$\left\{ \frac{\partial}{\partial t} + \psi_- \Omega_E \frac{\partial}{\partial \phi_-} - D_-^{\text{eff}} \frac{\partial^2}{\partial \phi_-^2} \right\} \langle \delta H(1) \delta H(2) \rangle = S_2. \tag{2.38}$$

Here, η is the ballooning angle coordinate that represents a position along a magnetic field line. The poloidal magnetic flux ψ and the toroidal angle ϕ play roles of the radial and the binormal coordinates, respectively. The orthogonal magnetic coordinates are shown in Fig. 2.1. Radial shear of the angular rotation

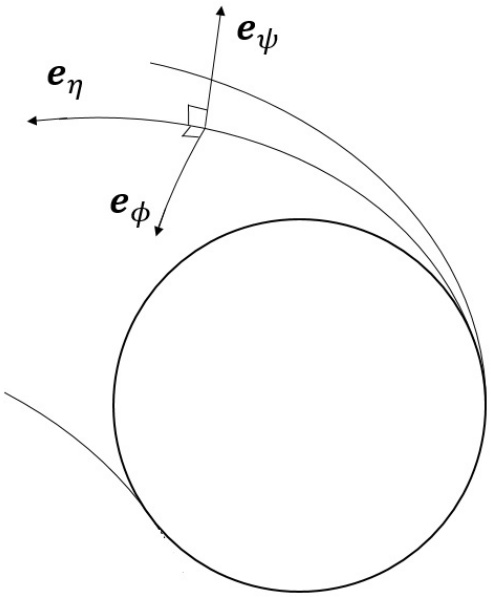

Figure 2.1 Orthogonal magnetic coordinates.

frequency associated with the mean E×B flow is given by

$$\Omega_E \equiv -\frac{\partial^2}{\partial\psi^2}\Phi_0\left(\psi\right) = \frac{\partial}{\partial\psi}\left(\frac{E_r^{(0)}}{RB_\theta}\right). \tag{2.39}$$

S_2 is the renormalized source term for the two-point correlation function. At small separation, the relative diffusion D_-^{eff} has the following asymptotic form for an untilted eddy [7, 8, 10, 11],

$$\frac{D_-^{\text{eff}}}{2D^{\text{eff}}} = \left(\frac{\psi_-}{\Delta\psi_0}\right)^2 + \left(\frac{\phi_-}{\Delta\phi_0}\right)^2 + \left(\frac{\eta_-}{\Delta\eta}\right)^2. \tag{2.40}$$

This characterizes the relative diffusion of two points inside a turbulence eddy with ellipsoidal shape. Here, $\Delta\psi_0/RB_\theta$, $RB_\theta\Delta\phi/B$ and $qR\Delta\eta$ are correlation lengths in the radial, binormal and along-the-field line directions, respectively. Note that D^{eff} is the diffusion coefficient at large separation in the binormal angle ϕ and therefore, has a dimension of frequency. This is related to a usual

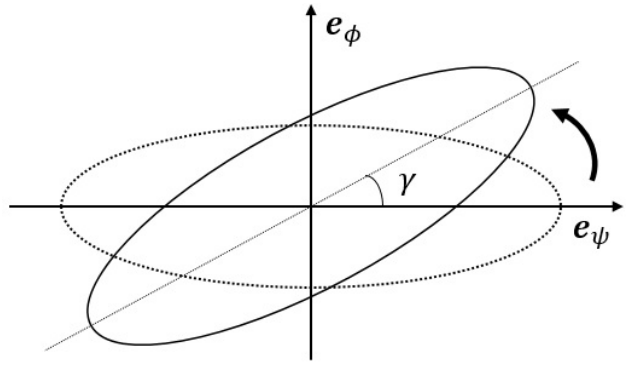

Figure 2.2 Initial tilting of an ellipsoidal eddy on a local radial-binormal plane. Here, γ is the initial tilting angle.

diffusion coefficient "D" via $D = (RB_\theta/B)^2 D^{\rm eff}$. Now, I present a form of $D_-^{\rm eff}$ appropriate to an initially tilted eddy. Here, we consider flute-like fluctuations, i.e., $\Delta\eta \to \infty$. Initial tilting of a turbulence eddy is represented by a rotation on a local radial-binormal plane, as shown in Fig. 2.2. Therefore, the form of relative diffusion for an initially tilted eddy is given by

$$\frac{D_-^{\rm eff}}{2D^{\rm eff}} = \frac{\psi_-^2}{(\Delta\psi_1)^2} + 2\frac{\psi_-\phi_-}{\Delta(\psi\phi)} + \frac{\phi_-^2}{(\Delta\phi_1)^2}. \tag{2.41}$$

The new characteristic scales in radial and binormal direction for the tilted eddy, $\Delta\psi_1$ and $\Delta\phi_1$, are expressed as

$$\Delta\psi_1 = \frac{\Delta\psi_0}{\left[e^2\sin^2\gamma + \cos^2\gamma\right]^{1/2}}, \tag{2.42}$$

$$\Delta\phi_1 = \frac{\Delta\phi_0}{\left[e^{-2}\sin^2\gamma + \cos^2\gamma\right]^{1/2}}. \tag{2.43}$$

Note that these are projections of an eddy boundary (in the absence of a mean E×B flow) in radial and binormal directions, respectively, and are proper quantifications obtained as a result of rotational transformation. Here, γ is the initial tilting angle which should not be confused with the ballooning angle measured

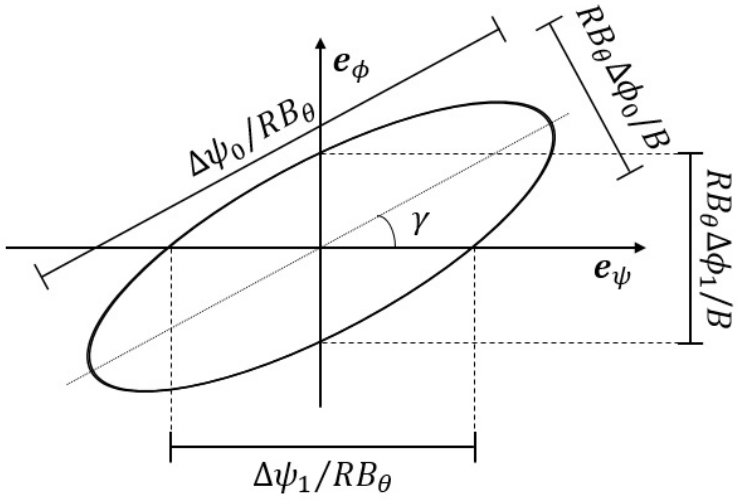

Figure 2.3 Characteristic scales representing structure of an initially tilted eddy.

from the midplane or a linear growth rate, and

$$e = \frac{\Delta\psi_0/RB_\theta}{RB_\theta\Delta\phi_0/B} \tag{2.44}$$

is elongation of the eddy along the principal axes. The characteristic scale of the cross-term $\Delta(\psi\phi)$ is

$$\Delta(\psi\phi) = \frac{\Delta\psi_0\Delta\phi_0}{(e - e^{-1})\sin\gamma\cos\gamma}. \tag{2.45}$$

The characteristic scales introduced above are shown in Fig. 2.3. Note that for an initially tilted eddy, $\Delta\psi_0$ and $\Delta\phi_0$ are no longer characteristic scales in radial and binormal direction. They are characteristic scales along principal axes.

2.5 Decorrelation of an initially tilted turbulence eddy in the presence of E×B shear

We investigate the decorrelation dynamics that comes from the coupling of the E×B flow shear and turbulent diffusion by following time-evolution of various

moments of the left hand side (LHS) of Eq. (2.38),

$$\partial_t \left\langle \psi_-^2 \right\rangle = 0, \tag{2.46}$$

$$\partial_t \left\langle \phi_-^2 \right\rangle = 4D^{\text{eff}} \left\{ \frac{\left\langle \psi_-^2 \right\rangle}{\Delta\psi_1^2} + 2\frac{\langle \psi_-\phi_- \rangle}{\Delta(\psi\phi)} + \frac{\left\langle \phi_-^2 \right\rangle}{\Delta\phi_1^2} \right\} + 2\Omega_E \langle \psi_-\phi_- \rangle , \tag{2.47}$$

$$\partial_t \langle \psi_-\phi_- \rangle = \Omega_E \left\langle \psi_-^2 \right\rangle . \tag{2.48}$$

Here, the average over turbulent trajectories is

$$\langle A(\eta_-, \phi_-, \psi_-) \rangle \equiv$$
$$\int d\eta'_- d\phi'_- d\psi'_- G\left(\eta_-, \phi_-, \psi_- | \eta'_-, \phi'_-, \psi'_-\right) A\left(\eta'_-, \phi'_-, \psi'_-\right), \tag{2.49}$$

where G is the Green's function for LHS of Eq. (2.38). Note that my theoretical model which is based on the ballooning mode formalism does not include relative turbulent diffusion in the radial direction as seen in Eq. (2.46). Nevertheless, this choice of fluctuation representation makes the geometric dependence of the E×B shearing rate most transparent [10–12] and serves the specific purpose of this study. Coupling of the E×B flow shear and turbulent diffusion in binormal direction as described in Eq. (2.47) and (2.48) provides us a crucial information which is sufficient for quantifying the effect of initial tilting of an eddy. Integration of Eq. (2.46) through Eq. (2.48) yields the following asymptotic expression for $\Delta\omega_T t > 1$:

$$\begin{aligned} \frac{\left\langle \phi_-^2 \right\rangle}{\Delta\phi_1^2} = \Bigg[& \frac{\psi_-^2}{\Delta\psi_1^2} \left\{ 1 + 2\frac{\Delta\psi_1^2}{\Delta\phi_1^2}\frac{\Omega_E^2}{\Delta\omega_T^2} + 2\frac{\Delta\psi_1^2}{\Delta(\psi\phi)}\frac{\Omega_E}{\Delta\omega_T} \right\} \\ & + 2\frac{\psi_-\phi_-}{\Delta(\psi\phi)} \left\{ 1 + \frac{\Delta(\psi\phi)}{\Delta\phi_1^2}\frac{\Omega_E}{\Delta\omega_T} \right\} + \frac{\phi_-^2}{\Delta\phi_1^2} \Bigg] e^{\Delta\omega_T t}. \end{aligned} \tag{2.50}$$

Here, $\Delta\omega_T \equiv 4D^{\text{eff}}/\Delta\phi_1^2$ is the nonlinear decorrelation rate of ambient tubulence. Note that D^{eff}, being a diffusion coefficient in the binormal angle, has a dimension of a frequency. Eq. (2.50) yields eddy lifetime which is a function of

the initial separation between two nearby points,

$$\tau_{\text{eddy}} \simeq \Delta\omega_T^{-1} \ln\left([\cdots]^{-1}\right), \tag{2.51}$$

where $[\cdots]$ is the expression multiplying $e^{\Delta\omega_T t}$ on RHS of Eq. (2.50). Recall that Eq. (2.41) implies $[\cdots] < 1$. In Eq. (2.51), logarithmic divergence of the eddy lifetime at small separation is a well-known property from two-point analyses. The eddy boundary shape across the magnetic field is given by an expression obtained by setting the argument of the natural logarithm, $[\cdots]$ equal to unity.

A key result of this study is obtained by examining the term multiplying $\psi_-^2/\Delta\psi_1^2$ in the argument of the natural logarithm in Eq. (2.51). In the terms multipling $\psi_-^2/\Delta\psi_1^2$ in Eq. (2.50), it is obvious that both the E×B shear (proportional to Ω_E) and an initial eddy tilting (contributes as $\Delta(\psi\phi)$) modify the range of initial radial separation of two nearby points (ψ_-) inside the eddy for which they are correlated. In Eq. (2.50), $2\psi_-\phi_-/\Delta(\psi\phi)$ represents initial eddy tilting, and $2(\psi_-\phi_-/\Delta\phi_1^2)\Omega_E/\Delta\omega_T$ represents eddy rotation due to E×B shear. We note a sign dependency of the eddy rotation. Rotation of an initially tilted eddy due to E×B shear can either add up to or subtract from an initial tilting, depending on signs of $\Delta(\psi\phi)$ and Ω_E, i.e., signs of the initial tilting angle and the E×B shear.

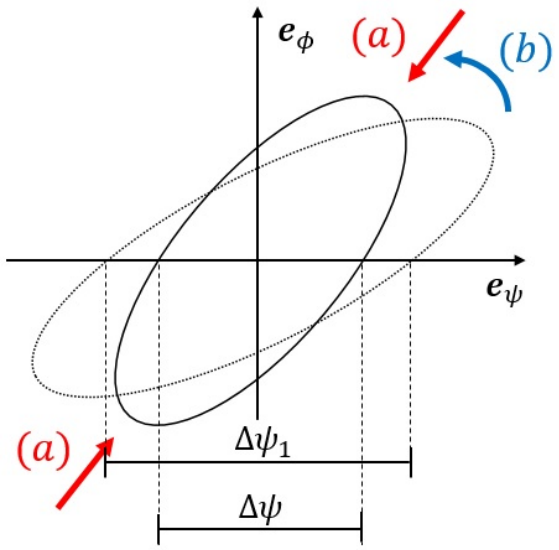

Figure 2.4 Radial width change of an eddy is a consequence of two E×B shear effects: (a) intrinsic scale reduction, and (b) eddy rotation.

2.6 Synergism between initial eddy tilting and E×B shear in turbulence suppression

From Eq. (2.50) and (2.51), an expression for boundary of an E×B-distorted eddy is given by

$$\frac{\psi_-^2}{\Delta\psi_1^2}\left\{1+2\frac{\Delta\psi_1^2}{\Delta\phi_1^2}\frac{\Omega_E^2}{\Delta\omega_T^2}+2\frac{\Delta\psi_1^2}{\Delta(\psi\phi)}\frac{\Omega_E}{\Delta\omega_T}\right\} + 2\frac{\psi_-\phi_-}{\Delta(\psi\phi)}\left\{1+\frac{\Delta(\psi\phi)}{\Delta\phi_1^2}\frac{\Omega_E}{\Delta\omega_T}\right\}+\frac{\phi_-^2}{\Delta\phi_1^2}=1, \tag{2.52}$$

and the radial width of the E×B-distorted eddy, $\Delta\psi$, is identified as

$$\frac{\Delta\psi_1^2}{\Delta\psi^2}=1+2\frac{\Delta\psi_1^2}{\Delta\phi_1^2}\frac{\Omega_E^2}{\Delta\omega_T^2}+2\frac{\Delta\psi_1^2}{\Delta(\psi\phi)}\frac{\Omega_E}{\Delta\omega_T}. \tag{2.53}$$

Fig. 2.4 illustrates change in the radial width of an initially tilted eddy due to E×B shear. Recall that we quantified the radial width of an eddy as a projection

of the eddy in radial direction. This radial projection changes from $\Delta\psi_1$ to $\Delta\psi$ due to combined effect of intrinsic scale reduction and rotation, in the presence of E×B shear. For an initially untilted eddy, Eq. (2.53) reduces to

$$\frac{\Delta\psi_1^2}{\Delta\psi^2} = 1 + 2\frac{\omega_{\rm HB}^2}{\Delta\omega_T^2}, \tag{2.54}$$

Here, we follow the definition of the E×B shearing rate in [11] as follows.

$$\omega_{\rm HB} \equiv \frac{\Delta\psi_0}{\Delta\phi_0}\Omega_E = e\frac{(RB_\theta)^2}{B}\frac{\partial}{\partial\psi}\left(\frac{E_r^{(0)}}{RB_\theta}\right) \tag{2.55}$$

This expression [3] explicitly shows more effective E×B shearing for a radially elongated eddy. The appearance of a factor of 2 in Eq. (2.54) is different from Eq. (17) of Ref. [11]. This difference is originated from different geometric characterizations of an eddy, not from an algebraic mistake. We note that in the absence of initial tilting ($\gamma = 0$), we can write Eq. (2.52) as

$$\frac{\psi_-^2}{\Delta\psi_1^2}\left\{1 + \left(\frac{\Delta\psi_1}{\Delta\phi_1}\frac{\Omega_E}{\Delta\omega_T}\right)^2\right\} + \frac{1}{\Delta\phi_1^2}\left(\phi_- + \frac{\Omega_E}{\Delta\omega_T}\psi_-\right)^2 = 1, \tag{2.56}$$

following Ref. [11]. This expression has a nice property of decoupling two effects of the E×B shear naturally. The first term on LHS describes a reduction of eddy size in the radial principal axis direction and the second term on LHS describes a distortion of an eddy shape due to a rotation of the other principal axis (originally in the binormal direction in the absence of E×B shear). Ref. [11] did not address the consequences of the eddy shape distortion, and utilized an expression of the first term on LHS only in characterizing the eddy size reduction in radial direction. In the presence of an initial eddy tilting characterized by a finite $\Delta(\psi\phi)$, Eq. (2.52) can no longer be factorized in a similar illuminating fashion as done in Ref. [11]. Furthermore, simultaneously addressing the eddy tilting (with its shape preserved) and the distortion of eddy shape could

be extremely complicated, if not confusing. Therefore, we take a more straightforward, if not elegant, approach of using the change in projected dimension of eddy size as described by Eq. (2.53). We also note that Eq. (2.53) predicts a turbulence eddy size reduction due to the E×B shear, not a full elimination of turbulence, like the previous nonlinear decorrelation theories [8, 10–12]. The emphasis of this study is the dependence of the E×B flow shear effects on the turbulence eddy's shape including its initial tilting angle. With this in mind, for a proper comparison to the result of Ref. [11], we simply take the following expression as a new criterion for E×B shear suppression of an initially tilted eddy.

$$\frac{\Delta\psi_1^2}{\Delta\phi_1^2}\frac{\Omega_E^2}{\Delta\omega_T^2} + \frac{\Delta\psi_1^2}{\Delta(\psi\phi)}\frac{\Omega_E}{\Delta\omega_T} > 1. \tag{2.57}$$

From Eq. (2.42) and (2.45), it becomes

$$\frac{e^{-2}\sin^2\gamma + \cos^2\gamma}{e^2\sin^2\gamma + \cos^2\gamma}\frac{\omega_{\rm HB}^2}{\Delta\omega_T^2} + \frac{(e - e^{-1})\sin\gamma\cos\gamma}{e^2\sin^2\gamma + \cos^2\gamma}\frac{\omega_{\rm HB}}{\Delta\omega_T} > 1. \tag{2.58}$$

This connects to the result of Ref. [11] in the limit of $\gamma \to 0$,

$$\frac{|\omega_{\rm HB}|}{\Delta\omega_T} > 1. \tag{2.59}$$

Hereafter, we set ranges of initial tilting angle γ and elongation e of an eddy as

$$-\frac{\pi}{2} < \gamma \le \frac{\pi}{2} \quad \text{and} \quad 1 \le e \tag{2.60}$$

for a definitive analysis for radially elongated tokamak turbulence eddies. Note that $\sin\gamma$ has the same sign as γ, while $\cos\gamma$ is always positive with our setting. If $e = 1$, we recover the E×B shear suppression criterion from Ref. [11], since there is no difference between an initially tilted eddy and an untilted eddy in this case. For $e > 1$, the criterion become

$$\left(\frac{\omega_{\rm HB}}{\Delta\omega_T} - f_+\right)\left(\frac{\omega_{\rm HB}}{\Delta\omega_T} - f_-\right) > 0, \tag{2.61}$$

where

$$f_{\pm} \equiv -\frac{1}{2}\frac{(e-e^{-1})\sin\gamma\cos\gamma}{e^{-2}\sin^2\gamma+\cos^2\gamma} \pm \sqrt{\left(\frac{1}{2}\frac{(e-e^{-1})\sin\gamma\cos\gamma}{e^{-2}\sin^2\gamma+\cos^2\gamma}\right)^2+\frac{e^2\sin^2\gamma+\cos^2\gamma}{e^{-2}\sin^2\gamma+\cos^2\gamma}}. \tag{2.62}$$

Note that f_+ is always positive and f_- is always negative, regardless of the sign of γ. Therefore, the following inequalities should be satisfied for the E×B shear suppression of an initially tilted eddy;

$$\frac{\omega_{\rm HB}}{\Delta\omega_T} > f_+ > 0 \quad \text{or} \quad \frac{\omega_{\rm HB}}{\Delta\omega_T} < f_- < 0. \tag{2.63}$$

Comparing f_+ with 1 and f_- with -1, we find the dependency of the E×B shear suppression on relative sign betweeen $\omega_{\rm HB}$ and γ. If $\omega_{\rm HB}$ and γ have same signs, the suppression is more effective than that of an untilted eddy for $0 < |\gamma| < \gamma_c$, where $\gamma_c \equiv \arctan\left[1/(e+e^{-1})\right]$. The suppression is less effective for $\gamma_c < |\gamma|$. Meanwhile, if $\omega_{\rm HB}$ and γ have opposite signs, the suppression is less effective in general. Here the radial width of the eddy can be even extended for a weak E×B shear $|\omega_{\rm HB}| < \omega_c$, where $\omega_c \equiv \left|(e-e^{-1})\sin\gamma\cos\gamma/(e^{-2}\sin^2\gamma+\cos^2\gamma)\right|\Delta\omega_T$.

In understanding synergistic effect between E×B shear and initial eddy tilting presented above, one should note that the radial width of an E×B-distorted eddy is always smaller than $\Delta\psi_0/RB_\theta$, which corresponds to the radial width of an untilted eddy in the absence of the E×B shear. Therefore, E×B-shear-distorted eddies always lead to weaker radial transport than untilted eddies in the absence of E×B shear.

Fig. 2.5 and 2.6 illustrate directions of E×B shear and initial eddy tilting. To understand this qualitative difference depending on the relative sign of $\omega_{\rm HB}$ and γ, one should recall that E×B shear influences radial width of an eddy via a combination of intrinsic scale reduction and rotation, as illustrated in Fig. 2.4.

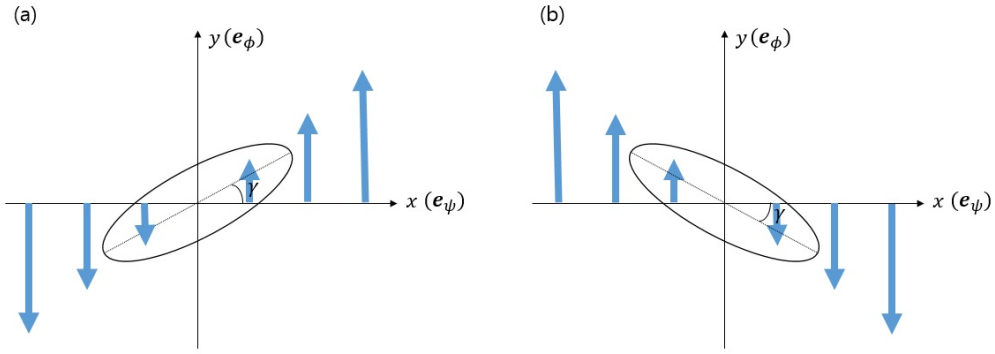

Figure 2.5 Illustration of E×B shear and initial eddy tilting for (a) $\omega_{\mathrm{HB}} > 0$ and $\gamma > 0$, (b) $\omega_{\mathrm{HB}} < 0$ and $\gamma < 0$.

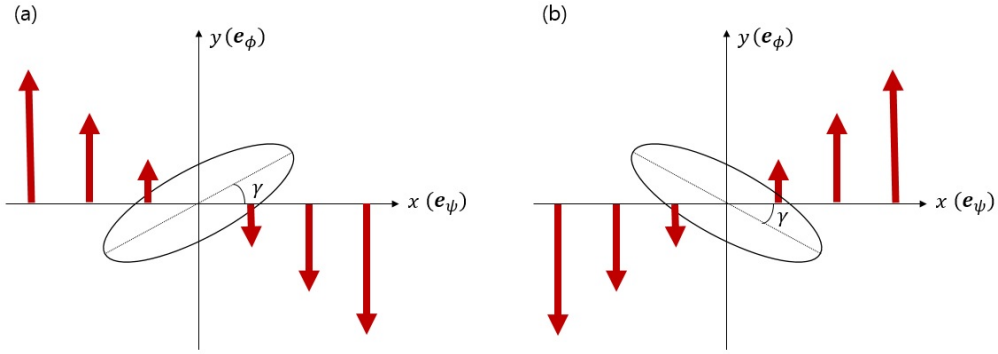

Figure 2.6 Illustration of E×B shear and initial eddy tilting for (a) $\omega_{\mathrm{HB}} < 0$ and $\gamma > 0$, (b) $\omega_{\mathrm{HB}} > 0$ and $\gamma < 0$.

For same signs of ω_{HB} and γ, which is illustrated in Fig. 2.5, positive synergy between E×B shear and initial eddy tilting happens. Here, the eddy rotates in the direction reinforcing initial tilting, and thus E×B shear induced scale reduction and rotation add up to reduce the radial width of the eddy. In this case, for small amount of initial tilting, E×B shearing is more effective compared to the case of an initially untilted eddy. It is expected that the optimum value of initial eddy tilting for positive synergism is small, since it is hard to rotate an eddy which is already tilted very much. Therefore, for large amount of initial eddy tilting, the E×B shear suppression is not that effective compared to the case of an initially untilted eddy.

On the other hand, it is obvious that the opposite signs of ω_{HB} and γ, which is illustrated in Fig. 2.6, is undesirable for effective E×B shearing. For small amount of initial tilting, E×B eddy rotation is in the direction reducing eddy tilting. Therefore, E×B shear suppression is less effective since eddy rotation tends to increase the radially projected eddy size, while scale reduction tends to reduce it. For large amount of initial tilting, the negative effect of eddy rotation can be larger than the effect of scale reduction, and thus radially projected eddy size can increase for a weak E×B shear. Note that for a given eddy elongation e, the critical E×B shearing rate ω_c increases as the absolute value of initial tilting angle $|\gamma|$ increases, so it is easier to extend eddy size for larger amount of initial tilting.

2.7 Applications and Discussion

Among various origins of initial eddy tilting, the most robust and important one is magnetic shear. There have been previous works illustrating the effect of magnetic shear on tilting of turbulence eddies. Ref. [26] suggested a sim-

ple eddy tilting model in the presence of magnetic shear in toroidal geometry with circular cross section, to explain stabilizing influence of negetive magnetic shear. A clear dependence of transport level on the sign of toroidal rotation velocity shear is observed in JT-60U [27] for negative shear plasmas. This observation agrees with my prediction of dependence of turbulence suppression and turbulent transport level on the sign of E×B shear.

A more recent model of magnetic shear induced eddy tilting near separatrix of single-null diverted plasmas [28] can be applied together with my theory to provide an explanation for well-known but not fully understood experimental observations of up-down asymmetry of H-mode transition power threshold [29]. In single null diverted plasmas, H-mode transition power threshold depends on direction of ion grad-B drift with respect to the location of X-point. When direction of ion grad-B drift is toward X-point (favorable), the transition power threshold is significantly lower than that in the opposite case (unfavorable). According to the model in Ref. [28], turbulence amplitude is relatively small in the vicinity of X-point so that eddies in the opposite side of X-point represent turbulence properties near separatrix. Since eddies are tilted toward low-field-side (LFS) midplane with positive magnetic shear [26, 28], the representative direction of magnetic shear induced eddy tilting is different for upper- and lower-single null diverted plasmas. Noting that radial electric field profile forms a well structure in edge and that H-mode transition starts at separatrix [30], my theory predicts more efficient E×B shear suppression for the favorable case. This can be an underlying physics of up-down asymmetry of H-mode transition power threshold. Fig. 2.7 shows a cartoon illustrating our explanation.

To demonstrate robustness of our mechanism on up-down asymmetry of H-mode transition threshold, I suggest measurement of turbulence decorrelation

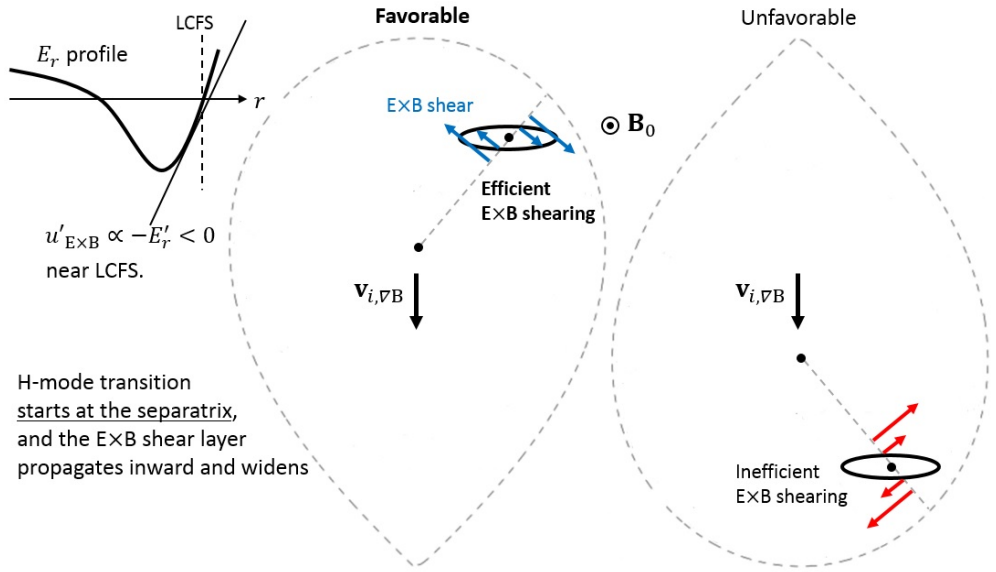

Figure 2.7 Illustration of up-down asymmetric E×B shearing near separatrix.

rate, profiles and turbulence eddy shapes near separatrix with high temporal resolution (∼1 ms) around H-mode transition. Turbulence decorrelation rate has frequently been approximated by maximal linear growth rate in estimating significance of the E×B shear suppression, but direct measurement of the decorrelation rate for instance via beam emission spectroscopy (BES) [31,32] is desirable for a more clear demonstration. E×B shearing rate can be calculated using radial force balance with measured profiles of ion pressure and flow velocities via fast charge-exchange recombination spectroscopy (CES) [33,34] and of magnetic field via motional stark effect (MSE) [35,36]. Alternatively, direct measurement of E×B velocity profile is available via Doppler back-scattering (DBS) [30,37] or gass-puff imaging (GPI) [38,39]. In addition to decorrelation rate and E×B shearing rate, information of eddy tilting angle and elongation is desirable for a quantitative validation of our theory. These can be measured via BES, GPI, or recently developed fast sweeping reflectometry [40] or correlation

Doppler reflectometry [41].

One should be aware that there exist other mechanisms explaining the up-down asymmetry of H-mode transition power threshold in single null diverted plasmas. An important one is effect of cross-field neoclassical (i.e., collisional) flux in scrape-off layer (SOL) induced by temperature gradient along the open magnetic field line [42]. For the case of single null diverted plasmas having favorable configuration, direction of the neoclassical flux is inward, giving additional heating power to the confined plasma inside last closed flux surface (LCFS), so that it enables H-mode transition with low external heating power [43]. For the unfavorable case, direction of the neoclassical flux is outward, so that it plays the opposite role. There are experimental observations that impurities in SOL can significantly enhance the poloidal temperature gradient and consequent radial neoclassical flux [44]. Impurities can have strong asymmetries in their deposition [45, 46] which result in enhancement of up-down asymmetry of H-mode transition power threshold by the radial neoclassical flux. There also exist a mechanism which emphasizes effect of parallel current in SOL, having different direction depending on the X-point location, on stability of resistive ballooning mode turbulence [47]. Note that these mechanisms are not competing ones with ours, since they are not on asymmetry of positive feedback loop toward transport barrier formation that I am focusing on. They can make synergistic effect together with our mechanism in enhancing up-down asymmetry of H-mode transition threshold. A series of experiments changing edge magnetic shear while keeping other parameters the same enable to validate robustness of our mechanism. Especially, it is desirable to keep edge pressure gradients the same to focus on our mechanism suggested in this section, since diamagnetic flows also affect initial eddy tilting [48, 49], while I want to focus on effect of magnetic shear.

This study has only addressed the effect of the flow shear on tilted turbulence eddies. On the other hand, it has been known that the zonal flows can be generated by Reynolds stress exerted by turbulence [50], in particular via collective tilting of turbulence eddies in one preferrential direction [51]. Our results seem to support this mechanism since the sum of zonal flow energy and ambient turbulence energy should be conserved. More efficient turbulence reduction for the same direction of tilting and zonal flow shear implies more efficient energy transfer from turbulence to the zonal flows i.e., flow generation. This feedback loop will certainly amplify for this case. Indeed, there is a study suggesting effect of different magnitude of E×B shear on the up-down asymmetry of H-mode transition threshold due to different Reynolds stress depending on the position of X-point [28]. The ratio of E×B shearing rate to turbulence decorrelation at the beginning of H-mode transition calculated using experimentally measured quantities would definitely separates effect of efficiency of E×B shear suppression to this one. Recall that our theory predicts that its magnitude at transition would be lower for the favorable case than that for the unfavorable case.

In conclusion, I have derived the E×B shear suppression criterion of turbulence for initially tilted eddies. Two point nonlinear analysis shows that initial eddy tilting in the same direction as the E×B shear can make the E×B shear suppression of turbulence more efficient compared to the no initial eddy tilting case when the initial tilting angle is not too large. Meanwhile, the initial tilting in the opposite direction with respect to the E×B shear makes the shearing less efficient in general. This relative sign dependency is more pronounced for highly elongated eddies.

Chapter 3

Shear suppression of trapped electron turbulence

Thorough understanding of transport barrier formation mechanism remains to be one of important issues in magnetic fusion research for several decades. Edge transport barrier and internal transport barrier (ITB) formation accompanied by drastic reduction of local turbulent transport leads to spontaneous transition to enhanced confinement regimes with improved performance of tokamak plasmas [52–59]. With abundant experimental evidences [1], E×B shear induced turbulence suppression [8, 10, 11] is widely accepted as a main mechanism of transport barrier formation. It is noteworthy that the E×B shear suppression is mostly mode independent and commonly applicable to various instabilities. This mechanism has worked well for density and ion thermal transport channels. On the other hand, for electron thermal ITB, reversed magnetic shear is most frequently mentioned as a necessary condition [60–64]. However, effects of the reversed shear configuration are mode dependent and less universal [65].

The role of trapped-electron precession shear was previously studied [3, 66] to explain favorable effect of localized electron heating on reversed magnetic shear plasmas, noting parametric dependence of trapped-electron precession shear on electron temperature gradient and magnetic shear. Nevertheless, there exist examples which cannot be explained by any one of E×B shear, reversed magnetic shear or trapped-electron precession shear alone.

In this chapter, I present a theory of E×B shear and trapped-electron precession shear induced suppression of tokamak turbulence. After a short introduction to Lagrangian description of motions of a magnetically trapped particle, I perform a systematic derivation of a two-point equation for trapped electron turbulence based on modern bounce-kinetic formalism. I show through a moment analysis that both E×B shear and trapped-electron precession shear, which appear naturally in the derivation, participate in suppressing trapped electron turbulence [67–72, 74, 75, 163]. I obtain a new suppression criterion appropriate for trapped electron turbulence, which manifests that effects of the two fundamental mean convection shear can either add up or subtract depending on their relative sign. In addition to linear stabilization of turbulence, reversed magnetic shear can play a role in reducing turbulence nonlinearly by interplay with E×B shear and trapped-electron precession shear through a dependency of both quantities on $\partial B_\theta/\partial r$. Finally, I discuss applications of the result to offer explanations of broader range of experimental results on electron thermal ITB.

3.1 Bounce-center motion of trapped particles in the presence of mean radial electric field

In this section, I present bounce-center equations of motion for magnetically trapped particles in the presence of mean radial electric field as typically observed in internal transport barriers. Following previous works [76–83], we use the one-form mechanics and the Lie transformation theory [81] for rigorous derivation of bounce-center equations of motion. Details of the derivation are available from the references and I present only outlines and results relevant to my purpose.

The unperturbed guiding-center phase-space Lagrangian one-form in the presence of mean radial electric field is given by [78, 79],

$$\gamma_0 = \left(q\mathbf{A} + m\mathbf{u}_{\mathrm{E}} + mv_{\parallel}\mathbf{b}\right) \cdot d\mathbf{R} + \frac{\mu B}{\Omega} d\theta - h_0 dt, \tag{3.1}$$

where $\mathbf{R}$ is the guiding-center position, μ is the magnetic moment in the frame moving with mean E×B drift velocity $\mathbf{u}_{\mathrm{E}}$, $v_{\parallel}$ is the guiding-center parallel velocity, θ is the gyrophase angle and Ω is the gyro-frequency. h_0 is the unperturbed guiding-center Hamilonian $h_0 = q\Phi + \mu B + mv_{\parallel}^2/2 + mu_{\mathrm{E}}^2/2 + (\mu B/2\Omega)\mathbf{b}\cdot\boldsymbol{\nabla}\times\mathbf{u}_{\mathrm{E}}$, which includes the electrostatic potential energy $q\Phi$. Note that in Eq. (3.1), the contribution from gyromotion which is not of our main interest, is decoupled as the term $(\mu B/\Omega)d\theta$ from the guiding-center dynamics.

To concentrate on the bounce-center motion of magnetically trapped particles in toroidal geometry adequately, we eliminate the gyromotion contribution and adopt the Clebsch coordinates (α, β, s). Here, α and β represent the vector potential $\mathbf{A} = \alpha\boldsymbol{\nabla}\beta$ and the magnetic field $\mathbf{B} = \boldsymbol{\nabla}\alpha \times \boldsymbol{\nabla}\beta$ with a specified gauge, and s denotes distance along the magnetic field line. In this study, we assume that mean electrostatic potential Φ is a flux function, i.e., $\Phi = \Phi(\beta)$.

From now, we use the notations $y_1 = \beta$ and $y_2 = \alpha$ and the indices a and b which have values of 1 or 2.

After a series of a gauge transformation and Lie transformations [76,77], we obtain the bounce center Lagrangian one-form in the presence of an electrostatic perturbation,

$$\bar{\Gamma} = q\bar{Y}_2 d\bar{Y}_1 + m u_{\mathrm{Ea}}(\bar{\mathbf{Y}}) d\bar{Y}_a + \bar{J} d\bar{\Psi} - \left[\bar{H}_0(\bar{\mathbf{Y}}, \bar{J}) + q\delta\phi_{\mathrm{eff}}(\bar{\mathbf{Y}}, \bar{J})\right] dt, \tag{3.2}$$

where $(\mathbf{Y}, J, \Psi)$ are bounce-center variables. Here, $\mathbf{Y}$ is the bounce-center position which includes a deviation from the guiding-center position $\mathbf{y}$, and (J, Ψ) are the action-angle variables which characterize the bounce motion. An overbar is used to denote Lie-transformed variables which properly describe the bounce-center motion in the presence of perturbations. Here, $u_{\mathrm{Ea}}(\bar{\mathbf{Y}}) \equiv \mathbf{u}_E \cdot \partial\mathbf{R}/\partial\bar{Y}_a$ are components of the mean E×B drift, and $\delta\phi_{\mathrm{eff}}$ is the fluctuating electrostatic potential. The lowest order term of $\delta\phi_{\mathrm{eff}}$ is the bounce-averaged potential, and the higher order corrections which we don't keep in the rest of this work can be found in Ref. [76].

In axisymmetric toroidal geometry, we obtain equations of motion which correspond to the Euler-Lagrange equation of the bounce center Lagrangian.

$$\frac{d\bar{Y}_1}{dt} = \frac{\partial\delta\phi_{\mathrm{eff}}}{\partial\bar{Y}_2}, \tag{3.3}$$

$$\frac{d\bar{Y}_2}{dt} = -\frac{1}{q}\frac{\partial\bar{H}_0}{\partial\bar{Y}_1} + \frac{\partial\delta\phi_{\mathrm{eff}}}{\partial\bar{Y}_1}, \tag{3.4}$$

$$\frac{d\bar{\Psi}}{dt} = \omega_{\mathrm{b}}(\bar{Y}_2, \bar{J}) + q\frac{\partial\delta\phi_{\mathrm{eff}}}{\partial\bar{J}}, \tag{3.5}$$

$$\frac{d\bar{J}}{dt} = 0. \tag{3.6}$$

Note that contributions from the second term on RHS of Eq. (3.2) is neglected, which make only small differences of order $\mathcal{O}(\omega_{\mathrm{E\times B}}/\Omega)$ from Eqs. (3.3)-(3.6). Here, $\omega_{\mathrm{E\times B}}$ is the E×B shearing rate [11]. Eq. (3.3) shows that there is no radial

motion of a bounce-center at the lowest order in the absence of a perturbation. From Eq. (3.4), we note that the total precession drift of the bounce-center consists of contributions from the mean E×B drift and the magnetic drifts. Note that $d\bar{Y}_2/dt$ correponds to the time rate change of the toroidal angle position ζ in axisymmetric toroidal geometry, since $d\alpha = d\zeta - \nu d\theta$ and the bounce-average eliminates the lowest order poloidal motion. Here θ is the poloidal angle and $\nu(\beta, \theta)$ is the local safety factor. Therefore, following the conventional description of trapped particles in tokamaks [84], the lowest order toroidal precession motion of the bounce center can be written as

$$\dot{\bar{Y}}_{2,0} = \langle \dot{\alpha} \rangle_b = \dot{\zeta} = -\left\langle \frac{\partial \Phi}{\partial \beta} \right\rangle_b - \frac{\mu}{q} \left\langle \frac{\partial B}{\partial \beta} \right\rangle_b = \omega_E + \omega_{\rm pr}, \tag{3.7}$$

where $\omega_E = E_r/RB_\theta$ and $\omega_{\rm pr}$ are the toroidal angular frequencies corresponding to the precession due to E×B drift and that due to magnetic field inhomogeneity respectively. From now on, by the precession drift we only refer to that due to magnetic drifts related to $\omega_{\rm pr}$.

3.2 Two-point equation for trapped-electron clumps

In this section, I present a derivation of two-point equation appropriate to trapped electron turbulence from the bounce-kinetic Vlasov equation, and perform a moment analysis which yields a criterion for suppression of the trapped electron turbulence. From the results of the previous section, the bounce-kinetic Vlasov equation is obtained as [76]

$$\frac{\partial \bar{F}}{\partial t} + \frac{d\bar{Y}_1}{dt}\frac{\partial \bar{F}}{\partial \bar{Y}_1} + \frac{d\bar{Y}_2}{dt}\frac{\partial \bar{F}}{\partial \bar{Y}_2} = 0, \tag{3.8}$$

where $\bar{F}(\bar{\mathbf{Y}}, \bar{J}, \bar{\mu}, t)$ is the bounce-center distribution function that has no bounce-phase Ψ dependence. Note that the bounce-kinetic description applies only to turbulence with a characteristic frequency ω lower than a trapped-electron

bounce frequency $\omega_{b,e} = \epsilon^{1/2} v_{\rm Te}/qR$. Therefore, my theory, presented in this chapter, applies to TEM (trapped electron modes) and ITG (ion temperature gradient) modes, but not to higher frequency, shorter electron gyroradius scale ETG (electron temperature gradient) modes. ETG is believed to be more susceptible to reversed magnetic shear than the E×B shear [65]. Note that bounce-kinetics have been applied to gyrokinetic nonlinear simulations of tokamak turbulence as well [85,86]. We use the bounce-kinetic Vlasov equation for trapped electron turbulence to obtain an equation for time-evolution of the fluctuating non-adiabatic electron bounce-center distribution function δh,

$$\left[\frac{\partial}{\partial t} + (\omega_E + \omega_{{\rm pr},e})\frac{\partial}{\partial \alpha} + \delta \mathbf{v}_{\rm E}\cdot\boldsymbol{\nabla}\right]\delta h = S. \tag{3.9}$$

Here, S is the driving source of the turbulence. Here, a simple notation (β, α) is used instead of $(\bar{Y}_2, \bar{Y}_1)$, and overbars on bounce-center variables are dropped for convenience. The fluctuating non-adiabatic electron distribution function is defined as $\delta h = \delta f_e - (e\delta\phi_{\rm eff}/T_e)F_0$, where $\bar{F}_e = F_0 + \delta f_e$. A term $\delta \mathbf{v}_{\rm E}\cdot\boldsymbol{\nabla}\delta h = (\partial_1 \delta\phi_{\rm eff})(\partial_2 \delta h) + (\partial_2 \delta\phi_{\rm eff})(\partial_1 \delta h)$ represents the E×B nonlinearity. The role of the E×B nonlinearity becomes more transparent in the two-point equation. As in previous works [7–11, 23, 87], the two-point equation is derived by the two-point renormalization process, with the use of average and relative coordinates after a symmetrization with respect to $(\alpha_1, \beta_1, \epsilon_1)$ and $(\alpha_2, \beta_2, \epsilon_2)$, followed by an ensemble average,

$$\left[\frac{\partial}{\partial t} + \beta_-(\Omega_E + \Omega_\beta)\frac{\partial}{\partial \alpha_-} + \epsilon_-\Omega_\epsilon \frac{\partial}{\partial \alpha_-} - D_-^{\rm eff}\frac{\partial^2}{\partial \alpha_-^2}\right]\langle \delta h(1)\delta h(2)\rangle = S_2. \tag{3.10}$$

In this equation, the E×B nonlinearity is approximated by a relative turbulent diffusion $D_-^{\rm eff}$ along the perpendicular direction [7,9,23], which has the following asymptotic form at small separation:

$$D_-^{\rm eff} = 2D^{\rm eff}\left[\frac{\beta_-^2}{\Delta\beta_0^2} + \frac{\alpha_-^2}{\Delta\alpha^2}\right], \tag{3.11}$$

where $D^{\rm eff} = \Delta\omega_T \Delta\alpha^2/4$ is proportional to the turbulent diffusion at large separation. Here $\Delta\beta_0/RB_\theta$ and $(RB_\theta/B)\Delta\alpha$ are correlation lengths of the trapped-electron fluctuation in radial and binormal directions, in the absence of E×B shear and precession shear, respectively. As I explained in the previous chapter, the asymptotic behavior of the relative diffusion $D_-^{\rm eff}$ is a consequence of keeping both coherent mode couplings of waves and non-wave-like incoherent fluctuations [7,87]. We employed the ballooning formalism in magnetic coordinates for a natural representation of small-scale radially-localized fluctuations in toroidal geometry. Unless one considers higher order terms, the radial scattering which must be present physically does not appear in Eq. (3.10). Nevertheless, the nonlinear evolution of a turbulence eddy described by the scattering in binormal direction provides us enough information to estimate the reduction in radial correlation length [10, 11] and the eddy shape distortion [88] as shown in previous works on the related topic. S_2 is the two-point renormalized source. In Eq. (3.10), we used (ϵ, κ) as velocity space variables, instead of (μ, J), where ϵ is the particle energy and κ is the pitch-angle parameter, because physics interpretation is more straightforward in terms of ϵ and κ. Radial shear of the E×B drift and that of the trapped electron precession are given by

$$\Omega_E \equiv \frac{\partial}{\partial\beta}\omega_E(\beta) \tag{3.12}$$

and

$$\Omega_\beta \equiv \frac{\partial}{\partial\beta}\omega_{{\rm pr},e}(\beta,\epsilon). \tag{3.13}$$

The variation of the trapped electron precession frequency in energy is characterized by

$$\Omega_\epsilon \equiv \frac{\partial}{\partial\epsilon}\omega_{{\rm pr},e}(\beta,\epsilon). \tag{3.14}$$

The decorrelation properties of the two-point correlation can be studied by taking various moments of the relative variables. The moments, which properly

describe stochastic trajectories of the relative motion of two points in the phase-space, are defined as the relative quantities weighted by the Green's function of Eq. (3.10). Then, one obtain evolution equations for the second order moments from Eq. (3.10);

$$\partial_t \left\langle \beta_-^2 \right\rangle = 0, \tag{3.15}$$

$$\partial_t \left\langle \alpha_-^2 \right\rangle = 4D^{\text{eff}} \left[\frac{\left\langle \beta_-^2 \right\rangle}{\Delta\beta_0^2} + \frac{\left\langle \alpha_-^2 \right\rangle}{\Delta\alpha^2} \right] + 2\left(\Omega_E + \Omega_\beta\right) \left\langle \beta_- \alpha_- \right\rangle + 2\Omega_\epsilon \left\langle \alpha_- \epsilon_- \right\rangle, \tag{3.16}$$

$$\partial_t \left\langle \epsilon_-^2 \right\rangle = 0, \tag{3.17}$$

$$\partial_t \left\langle \beta_- \alpha_- \right\rangle = \left(\Omega_E + \Omega_\beta\right) \left\langle \beta_-^2 \right\rangle + \Omega_\epsilon \left\langle \beta_- \epsilon_- \right\rangle, \tag{3.18}$$

$$\partial_t \left\langle \beta_- \epsilon_- \right\rangle = 0, \tag{3.19}$$

$$\partial_t \left\langle \alpha_- \epsilon_- \right\rangle = \left(\Omega_E + \Omega_\beta\right) \left\langle \beta_- \epsilon_- \right\rangle + \Omega_\epsilon \left\langle \epsilon_-^2 \right\rangle. \tag{3.20}$$

These moment equations yield a solution which has the following asymptotic form for $\Delta\omega_T t > 1$,

$$\begin{aligned} \frac{\left\langle \alpha_-^2 \right\rangle}{\Delta\alpha^2} = \Bigg[\frac{\beta_-^2}{\Delta\beta_0^2} \left\{ 1 + \frac{\Delta\beta_0^2}{\Delta\alpha^2} \frac{\left(\Omega_E + \Omega_\beta\right)^2}{\Delta\omega_T^2} \right\} + \frac{1}{\Delta\alpha^2} \left(\alpha_- + \frac{\Omega_E + \Omega_\beta}{\Delta\omega_T} \beta_- \right)^2 \\ + 2 \frac{\Omega_\epsilon}{\Delta\omega_T} \frac{\epsilon_-}{\Delta\alpha} \left(\frac{\Omega_\epsilon}{\Delta\omega_T} \frac{\epsilon_-}{\Delta\alpha} + \frac{\alpha_-}{\Delta\alpha} \right) \Bigg] e^{\Delta\omega_T t}. \end{aligned} \tag{3.21}$$

Noting that maximal extent of the separation is $\left\langle \alpha_-^2 \right\rangle = \Delta\alpha^2$, one obtains the clump (phase-space granulation) lifetime from this equation as follows,

$$\tau_{\text{clump}} = \Delta\omega_T^{-1} \ln\left([\cdots]^{-1} \right), \tag{3.22}$$

where $[\cdots]$ is the expression multiplying $e^{\Delta\omega_T t}$ on RHS of Eq. (3.21). Note that $[\cdots] < 1$ is guaranteed from Eq. (3.11) and (3.21), and thus the clump boundary is defined as $[\cdots] = 1$, i.e.,

$$\begin{aligned} \frac{\beta_-^2}{\Delta\beta_0^2} \left\{ 1 + \frac{\Delta\beta_0^2}{\Delta\alpha^2} \frac{\left(\Omega_E + \Omega_\beta\right)^2}{\Delta\omega_T^2} \right\} + \frac{1}{\Delta\alpha^2} \left(\alpha_- + \frac{\Omega_E + \Omega_\beta}{\Delta\omega_T} \beta_- \right)^2 \\ + 2 \frac{\Omega_\epsilon}{\Delta\omega_T} \frac{\epsilon_-}{\Delta\alpha} \left(\frac{\Omega_\epsilon}{\Delta\omega_T} \frac{\epsilon_-}{\Delta\alpha} + \frac{\alpha_-}{\Delta\alpha} \right) = 1. \end{aligned} \tag{3.23}$$

As discussed in Ref. [9], the last term in LHS of Eq. (3.23) gives us the upper bound for the energy difference of two-point correlation, $\Delta\epsilon \sim \Delta\alpha/(\Omega_\epsilon/\Delta\omega_T)$. Trapped electrons within an energy range $\Delta\epsilon$ maintain their correlation and carry heat collectively. The first term in LHS of Eq. (3.23) contains information pertaining to the reduction of the radial correlation length, i.e.,

$$\frac{\Delta\beta_0^2}{\Delta\beta^2} = 1 + \frac{(\omega_{\mathrm{E\times B}} + \omega_{\mathrm{PS}})^2}{\Delta\omega_T^2}. \tag{3.24}$$

Recall that $\Delta\beta_0/RB_\theta$ is the radial correlation length in the absence of E×B shear and precession shear, and $\Delta\beta/RB_\theta$ is that in the presence of E×B shear and precession shear. This result indicates that fluctuation decorrelation occurs when the sum of the E×B shearing rate $\omega_{\mathrm{E\times B}}$ and the trapped electron precession shearing rate ω_{PS} exceeds the decorrelation rate of the ambient turbulence $\Delta\omega_T$, i.e.,

$$|\omega_{\mathrm{E\times B}} + \omega_{\mathrm{PS}}| > \Delta\omega_T. \tag{3.25}$$

The E×B shearing rate in general axisymmetric geometry [11] is defined as

$$\omega_{\mathrm{E\times B}} \equiv \frac{\Delta\beta_0}{\Delta\alpha}\Omega_E = \frac{\Delta\beta_0}{\Delta\alpha}\frac{\partial}{\partial\beta}\left(\frac{E_r}{RB_\theta}\right). \tag{3.26}$$

The trapped electron precession shearing rate is defined in a similar manner, but its expression is much more complicated. In high aspect ratio circular concentric tokamak geometry, after averaging over energy to focus on the overall behavior of thermal trapped electrons, the precession shearing rate is given by [3, 66]

$$\omega_{\mathrm{PS}} \equiv \frac{\Delta\beta_0}{\Delta\alpha}\Omega_\beta = -\frac{\Delta\beta_0}{\Delta\alpha}\frac{\partial}{\partial\beta}\left(\frac{T_e G(\kappa)}{eB_\theta R^2}\right), \tag{3.27}$$

where $G(\kappa)$ is a function representing pitch-angle dependence of the precession frequency that varies from 1 for deeply trapped particles to -1 for barely trapped particles [67, 84, 89]. Note that $G > 0$ for trapped electrons that can resonate with drift waves and drive the collisionless trapped electron mode (CTEM)

unstable. We note that if the trapped electron precession frequency does not vary in radius over a macroscopic length scale, a nondiffusive long-range electron thermal transport can occur [163]. Eq. (3.24) recovers the result of E×B shear decorrelation in Ref. [11] for $\omega_{\rm PS} = 0$, and the result of trapped electron precession shear decorrelation in Ref. [3] and [66] for $\omega_{\rm E\times B} = 0$.

3.3 Relevance to Experimental Results on Electron Thermal Internal Transport Barrier

It is commonly believed that E×B flow shear induced turbulence suppression is a key mechanism for the formation of ion thermal ITBs and particle ITBs, with plenty of supporting evidences [1]. Relevant generic nonlinear decorrelation theories exist for the mechanism [8, 10, 11]. Meanwhile, reversed magnetic shear configuration is frequently mentioned as a crucial factor for the formation of electron thermal ITBs [60–64]. However, related theoretical explanations are not as universal as that on E×B flow shear for ion thermal ITBs. So far, mode-specific mechanisms are mostly suggested for a reversed magnetic shear induced ITB formation: linear stabilization of specific instabilities [65] or non-overlap of linear eigenmodes of specific instabilities due to rare fraction of mode rational surfaces [90, 91].

While numerous supporting evidences are frequently quoted for the necessity of the reversed magnetic shear on electron thermal ITB formation, there exist some counter examples as well which show formation of electron thermal ITB in monotonic safety factor profiles [92–94]. I argue that by considering both trapped electron precession shear and E×B shear, we can come up with a better explanation of broad range of experimental observations regarding electron thermal-ITB formation [1, 56–59, 95–103].

For many experiments with electron thermal ITB, E×B shear is weak indeed. However for some experiments, E×B shear was not either measured or discussed at all. However, my theory suggests that E×B shear should be considered alongside the trapped electron precession shear. From a theoretical view, I emphasize that E×B shear induced turbulence decorrelation is a generic nonlinear mechanism independent of the linear instability types [8, 10, 11]. Its direct influence is the reduction of the radial correlation and the amplitude of both TEM-dominated and ITG-dominated turbulence. Therefore, it is possible that it influences both electron thermal ITB and ion thermal ITB formation. Moreover, an experimental result from TFTR on ERS transition condition [54] shows that reversed magnetic shear configuration is not a sufficient condition for electron thermal-ITB formation, and neutral beam heating (which leads to E×B shear via radial force balance relation) power beyond a threshold value is needed for the transition. It has been also observed that E×B shear is crucial in sustaining an ITB in TEM-dominated, neutral beam-heated reversed shear plasmas [104].

Trapped electron precession shear was previously proposed in Ref. [66] and [3] to explain formation of a strong electron thermal ITB in the presence of strong local electron heating and reversed magnetic shear configuration [56, 97, 105]. From the electron temperature gradient dependence of the precession shearing rate, one can expect a positive feedback loop toward formation of an electron thermal transport barrier. Note that higher electron temperature (gradient) induces more efficient suppression of trapped electron turbulence via precession shear which may lead to transport barrier formation in our point of view. An experiment relevant to the precession shear suppression can be found in Ref. [98] which reported a formation of electron thermal ITB in lower-hybrid-wave heated reversed shear plasmas, in the absence of neutral beam heating.

This result implies that electron thermal ITB can be formed without strong (initial) E×B shear, and with only local electron heating and reversed magentic shear. There was no ion thermal ITB in this case, and it is consistent with usual explanation for ion thermal-ITB formation via E×B shear suppression of ITG turbulence. Meanwhile, Ref. [99] and [100] showed that local electron heating, which is related to (initial) electron precession shear, is not necessary for electron thermal-ITB formation. From the experimental results of Refs. [98–100], it is obvious that neither E×B shear nor trapped electron precession shear alone can provide a complete explanation on electron thermal-ITB formation. Simultaneous consideration of both is needed for an explanation of broad range of phenomena. My theoretical results presented in previous sections provide it.

A key result of my two-point analysis is that from Eq. (3.25), the relative sign between E×B shear and precession shear as well as their magnitudes is important in suppressing trapped electron turbulence. This shows that the E×B shear and the precession shear can either reinforce or interfere with each other in reducing turbulence, depending on local plasma conditions. For detailed analysis, it is useful to decompose the E×B shear and the trapped electron precession shear. The E×B shearing rate and the precession shearing rate can be rewritten as

$$\omega_{\mathrm{E\times B}} = \frac{E_r}{B}\left[\frac{1}{E_r}\frac{\partial E_r}{\partial R} - \frac{1}{B_\theta}\frac{\partial B_\theta}{\partial R} - \frac{1}{R}\right] \tag{3.28}$$

and

$$\omega_{\mathrm{PS}} = -\frac{T_e G}{eBR}\left[\frac{1}{T_e}\frac{\partial T_e}{\partial R} - \frac{1}{B_\theta}\frac{\partial B_\theta}{\partial R} - \frac{2}{R}\right] \tag{3.29}$$

at the outer (i.e. low-field-side) midplane, with a typical approximation of an isotropic eddy shape in perpendicular plane [3] $(RB_\theta/B)\Delta\alpha \approx \Delta\beta_0/RB_\theta$. In this form, we note dependence of E_r and T_e themselves in determining E×B shear and precession shear, respectively. It should also be noted that the term

$B_\theta^{-1}\partial_R B_\theta$, which is related to magnetic shear, is important and can even dominate other terms of E×B shearing rate in the early stage of ITB formation with high power neutral beam injection (NBI) [57, 95]. Therefore, one should remember the contribution from magnetic shear in determining E×B shearing rate and precession shearing rate, in addition to that from E_r shear and T_e shear.

From the fact that magnetic shear either increases and decreases together with $-B_\theta^{-1}\partial_R B_\theta$, and that $T_e^{-1}\partial_R T_e$ is always negative at the outer midplane, one finds that reversed magnetic shear is preferred for an increase of precession shear. This may explain favorable role of reversed magnetic shear configuration in electron temperature ITB formation. The T_e-gradient dependence of precession shear allows a constructive feedback loop on suppression of trapped electron turbulence. Precession shear induced turbulence suppression steepens T_e-gradient, and accordingly enhanced precession shear suppresses the trapped electron turbulence more strongly. We also note that G depends on the magnetic shear $\hat{s}$. As $\hat{s}$ becomes more negative, more number of barely trapped particles can have $G < 0$ and precess in the opposite direction compared to the deeply trapped particles. This is well-known to be a linear stabilizing effect on CTEM by diminishing the wave-trapped electron precession resonance [89, 106, 107]. My theory presented in this thesis does not rely on the precession resonance, and seeks for the roles of magnetic shear via different mechanisms.

For E×B shear, the interplay between radial electric field (shear) and magnetic shear is much more complicated, since radial electric field profile varies much depending on specific experiments. For example, most of TFTR and JT-60U plasmas with ITB's where balanced-NBI or perpendicular-NBI is applied, exhibit E_r well structure. On the other hand, DIII-D results show E_r hill due

to co-NBI [108]. Precise calculation on E×B shear and precession shear using experimantal data from various discharges will clearly reveal influence of precession shear and its interplay with E×B shear on electron thermal-ITB formation. Another possible interplay between the E×B shear and the magnetic shear can occur through a momentum transport dependence on magnetic shear as demonstrated in lower hybrid current drive (LHCD) experiments in C-Mod [109] and as investigated by nonlinear gyrokinetic simulations [75,110,111]. However, this topic is beyond the scope of my study. In this work, I focused on presenting representative experimental examples on the synergism between E×B shear and precession shear instead of detailed case-by-case analysis, to illustrate general trends relevant to my theoretical predictions.

As previously mentioned, synergism between E×B shear and precession shear on suppression of trapped electron turbulence is determined by their relative sign. When the relative sign is positive, they reinforce each other to suppress turbulence strongly. If the relative sign is negative, they interfere with each other. As candidates of evidence, I draw attention to Ref. [101] for a constructive combination, and Ref. [102] and [103] for an interfering combination. Ref. [101] presents a JT-60U result on NB-heated reversed shear plasma which shows enhancement of electron thermal ITB by additional central electron cyclotron heating (ECH). With a typical radial electric field profile of JT-60U reversed shear plasmas which has a narrow well around the ITB foot [112,113], E×B shearing rate is expected to have a positive sign at the outer part of the radial electric field well. Expecting the average precession shearing rate for trapped particles is positive in that region, the experimental result suggests a constructive combination of E×B shear and precession shear in enhancing an electron thermal ITB. On the other hand, Ref. [102] presents a DIII-D experiment result on NB-heated reversed shear plasma, showing that central ECH in

addition to NBI heating can make confinement of electron heat worse compared to no-ECH case. Since a typical DIII-D reversed shear plasma has a radial electric field hill in the central region [108, 114], one expects E×B shearing rate to be negative in the ITB region. Therefore, the effects from E×B shear and precession shear can interfere with each other, and the increase of the amplitude of precession shearing rate due to central ECH could sometimes lead to a worse electron thermal confinement. Note, however, that this kind of degradation of ITB due to central electron heating is not always unfavorable, since one can control impurity accumulation inside ITB foot and avoid MHD instability-induced ITB collapse via controlled enhancement of TEM driven transport with central electron heating. This way of ITB control was performed in Alcator C-Mod [115] and analyzed with nonlinear gyrokinetic simulations [116,117]. Finally, Ref. [103] presents an experimental result from JT-60U which shows destructive effect of additional NBI on electron thermal ITB which has been initially formed by central ECH on reversed shear plasma. One could speculate that this is due to an adverse synergism between E×B shear and precession shear in the inner-half region of the radial electric field well inside the ITB foot point. These examples show that careful comparison between E×B shear and precession shear, considering their relative sign as well as their amplitudes, is necessary in analyzing and predicting electron thermal-ITB formation.

Along with the local turbulence suppression discussed so far, one should be aware that mitigation of nonlocal turbulent proparation could play a role in ITB formation as indicated by a few gyrokinetic simulations [118–120].

For an experimental observation of the interplay between E×B shear and precession shear on electron thermal ITB formation that my theory addresses, I suggest to focus on difference in start time of ITB formation between ion and

electron temperature channels. Note that the beginning of ITB formation is characterized by sudden reduction of turbulent fluctuation. In TEM-dominated plasmas, turbulent fluctuation of trapped electron distribution function plays an important role in electron thermal transport so that I expect clear difference in start time of ITB formation between ion and electron temperature channels. Recall that trapped electron precession shear appears only in the equation for trapped electron fluctuations. Meanwhile, in ITG mode-dmoinated plasmas, trapped electrons do not play an important role so that the channel dependence would be much weaker than that in the TEM-dominate plasmas. It is desirable to control safety factor profile to be similar in the two cases, to rule out effects from other mechanisms relying on reversed magnetic configuration as much as possible. To observe the features I expect, it is necessary to measure turbulent fluctuations of both ion and electron temperature near ITB foot. Ion temperature fluctuation can be measured e.g. via fast CES and electron temperature fluctuation via electron cyclotron emission (ECE) diagnostics [121–123]. Calculation of shearing rates using measured profiles with high time-resolution via fast CES and Thomson scattering [124] and comparison of them with measured value of turbulence decorrelation rate near the start time of ITB formation will clearly demonstrate robustness of my mechanism.

In summary, I developed a nonlinear theory on suppression of trapped electron turbulence, starting from modern bounce-kinetic formalism. Trapped electron precession shear, as well as E×B shear, is naturally included in the derivation of equation for two-point correlation. Result of my two-point analysis is applicable for a wide range of electron thermal ITB formation phenomena where any one of reversed magnetic shear, E×B shear or precession shear alone cannot provide a satisfactory explanation of them. Precession shear and E×B shear can either reinforce or interfere each other in reducing turbulence depending on

their relative sign, allowing us to explain various features of the electron thermal ITB formation.

Chapter 4

3D magnetic field effect on tokamak zonal flows

Large edge localized modes (ELMs) which are frequently observed in H-mode plasmas induce huge transient heat load on plasma facing components. Therefore, the ELM control is a critical issue for successful operation of International Thermonuclear Experimental Reactor (ITER) [125] and future fusion machines. It has been well demonstrated that externally imposed non-axisymmetric resonant magnetic perturbation (RMP) is a useful tool to mitigate or suppress the large ELMs in axisymmetric toroidal fusion machines [126–132]. On the other hand, application of RMPs causes increase of the L-H transition power threshold [133–137]. Theoretical and numerical studies [4] and experimental measurements [138, 139] have indicated that zonal flows can play a key role in triggering L-H transition. However, the RMP effect on zonal flows for L-H transition has not been explored in detail in toroidal geometry.

Motivated by these observations, I perform a theoretical study of the non-

axisymmetric (3D) magnetic field effect on zonal flows in tokamak plasmas using gyrokinetic equations, extending the previous works on axisymmetric tokamak [82,140] and Large Helical Device (LHD)-like stellarator [141,142]. In this work, I show that in the presence of a static 3D field, energy dependent secular radial drifts of particles induce velocity space phase-mixing of zonal mode distribution function. I show by an explicit calculation that this phase-mixing leads to a long-time asymptotic algebraic decay of zonal flows toward zero. The rate of the 3D field induced collsionless zonal flow decay is $\gamma_{3\mathrm{D}} = nqk_r\rho_{\mathrm{th}i}(v_{\mathrm{th}i}/R)(\delta_{m_0}/\epsilon)$, where n is the toroidal mode number of the RMP field, q is the safety factor, k_r is the zonal flow radial wavenumber, $v_{\mathrm{th}i}$ is the ion thermal speed, R is the distance from the major axis, and ϵ is the inverse aspect ratio. δ_{m_0} is the magnitude of the magnetic field strength variation due to the resonant component of the applied RMPs. In my work, the parallel (to the tokamak magnetic field) component of the RMP field $\delta B_{\|}$ directly contributes to the zonal flow decay, and the radial component δB_r have indirect influence via magnetic surface deformation. My result indicates lower zonal flow level and thus higher L-H transition power threshold in the presence of stronger RMP in tokamak plasmas. Previous theoretical works of RMP effect on zonal flows [143–145] have focused on roles of the radial component of the RMP field δB_r. In fact, most of analytic and numerical works regarding RMP effect on ELMs and confinement have been dedicated to roles of δB_r. An exception is a gyrokinetic simulation result in Ref. [146] where 3D MHD equilibria in the presence of RMP have been used. In this work, I study effects of the parallel component of the RMP field $\delta B_{\|}$ on tokamak edge plasmas.

4.1 Long-time behavior of zonal flows

To study zonal flow response to a source (from tokamak turbulence) in the presence of externally imposed 3D magnetic field, we consider a low-β circular concentric equilibrium in which a tokamak magnetic field and a (time-independent) helical 3D magnetic field have the following expressions.

$$\mathbf{B}_{\text{tokamak}} = \mathbf{B}_0 = \mathbf{e}_\theta B_\theta + \mathbf{e}_\zeta B_0/[1 + (r/R_0)\cos\theta], \tag{4.1}$$

$$\mathbf{B}_{\text{3D}} = \delta\mathbf{B} = \delta\mathbf{B}_\perp + \mathbf{b}_0\,\delta B_\parallel, \tag{4.2}$$

where $\mathbf{b}_0 \equiv \mathbf{B}_0/|\mathbf{B}_0|$ and $\delta\mathbf{B}_\perp = \mathbf{b}_0 \times (\delta\mathbf{B} \times \mathbf{b}_0)$. We assume a high aspect ratio tokamak, i.e., $r/R_0 \equiv \epsilon \ll 1$, and thus $B_\theta/B_0 \simeq \epsilon/q \ll 1$ with safety factor q of order unity. We consider a total magnetic field $\mathbf{B} = \mathbf{B}_0 + \delta\mathbf{B}$ having configuration of deformed magnetic surfaces. We use an ordering $|\delta\mathbf{B}_\perp/B_0| \sim \left|\delta B_\parallel/B_0\right| \sim \delta \ll 1$ for the 3D field [147] where the small parameter δ represents relative amplitude of the 3D field. In this work, we only consider toroidicity induced magnetic trapping and ignore other class of magnetic trapping, by assuming $\delta \ll \epsilon$ and moderate variation of the 3D field on the poloidal and the toroidal angle. This ordering is consistent with values from experiments [148]. In this work, we do not consider the toroidal field ripple which typically satisfies $N\delta \lesssim \epsilon$ [171] where N is toroidal mode number of the ripple. Furthermore, KSTAR reported an extremely low level of toroidal field ripple [150].

We use gyrokinetic equations for proper description of zonal flow response to a source [82, 140, 141, 151]. The gyrocenter distribution function is given by $f = F_0 + \delta f$, where F_0 and δf are the equilibrium and the perturbed distribution, respectively. The perturbed distribution is further divided into $\delta f = -(e\langle\phi\rangle_g/T)F_0 + g$. We consider electrostatic fluctuations in a low-β plasma. Here ϕ is the perturbed electrostatic potential, $\langle\cdots\rangle_g$ is gyroaverage

and using $g = g(\mathbf{R}, E, \mu, t)$ facilitates algebra. Here $\mathbf{R} \equiv \mathbf{x} - \boldsymbol{\rho}$ is the gyrocenter position, $\boldsymbol{\rho} = \mathbf{b} \times \mathbf{v}/\Omega$ is the Larmor radius, and $\Omega = eB/M$ is the gyrofrequency. $\mathbf{b} \equiv \mathbf{B}/|\mathbf{B}|$ is the unit vector along the total magnetic field line. We use the energy $E = Mv^2/2$ and the magnetic moment $\mu = Mv_\perp^2/2B$ as velocity variables. For an adequate description of zonal flows, we apply an eikonal representation which specifies rapid radial variation with $\phi(\mathbf{x}) = \phi_\mathbf{k} \exp[iS(\psi)]$ and similarly for $g(\mathbf{R})$. Here ψ is the poloidal magnetic flux, which acts as a flux surface label. The wave vector for zonal flows is $\mathbf{k} = \boldsymbol{\nabla} S(\psi)$. The gyrokinetic Vlasov equation for zonal flows is [140, 141]

$$\frac{\partial g_\mathbf{k}}{\partial t} + v_\parallel \mathbf{b} \cdot \boldsymbol{\nabla} g_\mathbf{k} + i\omega_\mathrm{D} g_\mathbf{k} = \frac{e}{T} F_0 J_0 \frac{\partial \phi_\mathbf{k}}{\partial t} + S_\mathbf{k}, \tag{4.3}$$

where $J_0 = J_0(k_r \rho)$ is the zeroth order Bessel function. Here the magnetic drift frequency is $\omega_\mathrm{D} = (\mathbf{v}_\mathrm{D} \cdot \boldsymbol{\nabla}\psi) S'(\psi)$, where $\mathbf{v}_\mathrm{D} = -v_\parallel \mathbf{b} \times \boldsymbol{\nabla}(v_\parallel/\Omega)$ is the magnetic drift velocity in low-β limit. The source term $S_\mathbf{k}$ comes from the $\mathbf{E} \times \mathbf{B}$ nonlinearity, and is responsible for the zonal flow generation by drift wave turbulence. The gyrokinetic Poisson equation, which determines the zonal flow potential $\phi_\mathbf{k}$, is approximated by the quasi-neutrality condition

$$-n_0 \frac{|e|\phi_\mathbf{k}}{T_i} + \int d^3v J_0 g_{i\mathbf{k}} = n_0 \frac{|e|\phi_\mathbf{k}}{T_e} + \int d^3v g_{e\mathbf{k}}, \tag{4.4}$$

where the small electron Larmor radius limit is used.

We consider long-time evolution of the zonal flows in a tokamak with 3D field. We choose F_0 to be Maxwellian in the remaining part of the paper. We solve the gyrokinetic Vlasov equation, Eq. (4.3), by assuming short bounce (and transit) time ($\omega_{\mathrm{b/t}} \gg \omega$). The leading order equation is

$$v_\parallel \mathbf{b} \cdot \boldsymbol{\nabla} g_0 + i\omega_{\mathrm{D}0} g_0 = 0. \tag{4.5}$$

Here we have decomposed the magnetic drift frequency as $\omega_\mathrm{D} = \omega_{\mathrm{D}0} + \overline{\omega}_\mathrm{D}$, where $\omega_{\mathrm{D}0}$ represents fast radial drift due to tokamak magnetic field, and $\overline{\omega}_\mathrm{D}$

represents slow secular radial drift of bounce-center due to 3D field [141]. Eq. (4.5) yields a solution of the form $g_0 = h\exp(-iQ)$, where $\mathbf{b}\cdot\boldsymbol{\nabla}h = 0$, and $Q \simeq (MI/e)S'(\psi)v_\parallel/B_0$ contains the finite orbit width (FOW) effect. Here $I \equiv RB_\zeta$. The next order equation in $\omega/\omega_{\rm b/t}$ expansion is

$$v_\parallel \mathbf{b}\cdot\boldsymbol{\nabla}g_1 + i\omega_{\rm D0}g_1 + i\overline{\omega}_{\rm D}g_0 = -\frac{\partial g_0}{\partial t} + \frac{e}{T}F_0 J_0 \frac{\partial \phi_{\mathbf{k}}}{\partial t} + S_{\mathbf{k}}. \tag{4.6}$$

Here, the effect of 3D field enters through $\overline{\omega}_{\rm D}$. If we consider an impulse source $S_{\mathbf{k}} = \delta f_{\mathbf{k}}(0)\delta(t)$, solving Eq. (4.6) becomes an initial value problem. Following a standard approach for ion gyroradius scale turbulence [140], we consider the ion source as $\delta f_{i\mathbf{k}}(0) = (\delta n_{i\mathbf{k}}(0)/n_0)(J_0/\Gamma_0)F_{i0}$ while neglecting the electron source, where $\delta n_{i\mathbf{k}}(0) = -\delta n_{i\rm pol} = n_0(1-\Gamma_0)e\phi_{\mathbf{k}}(0)/T_i$ and $\delta n_{i\rm pol}$ is the ion polarization density [152–154]. $\Gamma_0(k_\perp^2\rho_{{\rm th}i}^2)$ is defined as $\Gamma_0(x) \equiv e^{-x}I_0(x)$, where $I_0(x)$ is the zeroth order modified Bessel function. Note that the zonal flow response to a general source $S_{\mathbf{k}}$ can be readily obtained utilizing the form of the known impulse response [142]. After a bounce/transit orbit average, Eq. (4.6) yields

$$\frac{\partial h}{\partial t} = \frac{e}{T}F_0\overline{\left(e^{iQ}J_0\frac{\partial\phi_{\mathbf{k}}(t)}{\partial t}\right)} - i\overline{\omega}_{\rm D}h. \tag{4.7}$$

Its solution is

$$\begin{aligned} h(t) =& \overline{(e^{iQ}\delta f_{\mathbf{k}}(0))}e^{-i\overline{\omega}_{\rm D}t} + \frac{e}{T}F_0\overline{(e^{iQ}J_0\phi_{\mathbf{k}}(t))} \\ & - i\overline{\omega}_{\rm D}\int_0^t dt' e^{-i\overline{\omega}_{\rm D}(t-t')}\frac{e}{T}F_0\overline{(e^{iQ}J_0\phi_{\mathbf{k}}(t'))} \end{aligned} \tag{4.8}$$

after an integration by part. By definition, the initial value of $h(t)$ satisfies

$$h(0) = \overline{(e^{iQ}\delta f_{\mathbf{k}}(0))} + \frac{e}{T}F_0\overline{(e^{iQ}J_0\phi_{\mathbf{k}}(0))}. \tag{4.9}$$

Now we approximate the third term on the RHS of the Eq. (4.8) following Ref. [142]. We consider a characteristic time scale $\tau \sim \overline{\omega}_{\rm D}^{-1}$. In the short-time

limit $t \ll \tau$, the third term is negligible. In the long-time limit $t \gg \tau$, we note that net contribution of the integrand for time interval $0 < t' < t - \tau$ to the perturbed density becomes small due to the phase mixing in velocity space. Note that $\overline{\omega}_{\rm D}$ is velocity dependent. For time interval $t - \tau < t' < t$, we can replace $\phi(t')$ with $\phi(t)$ in the integrand. Therefore, the approximate solution applicable to both short-time and long-time limit is

$$h(t) \simeq \left[\overline{(e^{iQ}\delta f_{\mathbf{k}}(0))} + \frac{e}{T}F_0\overline{(e^{iQ}J_0\phi_{\mathbf{k}}(t))}\right] e^{-i\overline{\omega}_{\rm D}t}. \tag{4.10}$$

Substituting the solution into the quasi-neutrality condition yields

$$\mathcal{L}(t)\phi_{\mathbf{k}}(t) = I(t), \tag{4.11}$$

where

$$\begin{aligned}\mathcal{L}(t)\phi_{\mathbf{k}}(t) \equiv & n_0 e\left(\frac{1}{T_i} + \frac{1}{T_e}\right)\phi_{\mathbf{k}}(t) \\ & - \frac{e}{T_i}\int d^3v F_{0i} J_0 e^{-iQ}\overline{e^{iQ}J_0\phi_{\mathbf{k}}(t)}e^{-i\overline{\omega}_{{\rm D}i}t} \\ & - \frac{e}{T_e}\int d^3v F_{0e}\overline{\phi_{\mathbf{k}}(t)}e^{-i\overline{\omega}_{{\rm D}e}t}\end{aligned} \tag{4.12}$$

and

$$I(t) \equiv \int d^3v J_0 e^{-iQ}\overline{e^{iQ}\delta f_{i\mathbf{k}}(0)}e^{-i\overline{\omega}_{{\rm D}i}t} \tag{4.13}$$

taking small electron orbit width limit. For further analysis, we define an inner product by $(u, v) \equiv \langle u^* v\rangle$, where $\langle\cdots\rangle$ is the flux-surface average. Here we assume that geodesic acoustic modes and ion acoustic modes are already Landau damped, and take $\mathbf{b}\cdot\boldsymbol{\nabla}\phi_{\mathbf{k}} = 0$ [151]. From Eq. (4.11) we have $(\phi_{\mathbf{k}}(t), \mathcal{L}(t)\phi_{\mathbf{k}}(t)) = (\phi_{\mathbf{k}}(t), I(t))$, or

$$\frac{e\phi_{\mathbf{k}}(t)}{T_i} = \frac{\langle I(t)\rangle}{\mathcal{D}(t)}, \tag{4.14}$$

where the neoclassically enhanced polarization shielding is represented by

$$\mathcal{D}(t) \equiv \left\langle \int d^3v F_{0i} \left(1 - J_0 e^{-iQ} \overline{e^{iQ} J_0} e^{-i\overline{\omega}_{\mathrm{D}i} t}\right) \right\rangle + \frac{T_i}{T_e} \left\langle \int d^3v F_{0e} \left[1 - e^{-i\overline{\omega}_{\mathrm{D}e} t}\right] \right\rangle. \tag{4.15}$$

4.2 3D field induced zonal flow decay

In this section, I present an explicit calculation of the 3D magnetic field induced phase mixing of the zonal flow. Here we consider a single toroidal mode number (but multi-poloidal mode numbers) RMP field as a specific example of an explicit calculation. The factor $\exp\left(-i\overline{\omega}_{\mathrm{D}} t\right)$ in the integrands in Eq. (4.13) and (4.15) leads to a collisionless zonal flow decay in time as a consequence of phase mixing in velocity space. To begin with, we apply a perturbative treatment of the orbit average based on the Lagrangian variation of the magnetic field strength [155]. Instead of direct calculation of the magnetic field strength variation along a convoluted field line, we consider the magnetic surface deformation perturbatively on the position of an unperturbed field line as follows.

$$B(\mathbf{x}) = |\mathbf{B}_0(\mathbf{x}) + \delta\mathbf{B}(\mathbf{x})| \simeq |\mathbf{B}_0(\mathbf{x}_0)| + \delta_{\mathrm{L}} B(\mathbf{x}_0), \tag{4.16}$$

where $\delta_{\mathrm{L}} B$ is called the Lagrangian variation of the magnetic field strength and is given by

$$\delta_{\mathrm{L}} B(\mathbf{x}_0) = \mathbf{b}_0(\mathbf{x}_0) \cdot \delta\mathbf{B}(\mathbf{x}_0) + \boldsymbol{\xi} \cdot \boldsymbol{\nabla} B_0(\mathbf{x}_0). \tag{4.17}$$

Here $\mathbf{x} = \mathbf{x}_0 + \boldsymbol{\xi}$, where $\mathbf{x}_0$ is the position on an unperturbed magnetic field and $\boldsymbol{\xi}$ is the displacement of the magnetic field due to the 3D field. Note that here and hereafter we only perform perturbative analysis up to the first order in δ. As inferred from an approximate expression of the magnetic field strength, Eq. (4.16) and (4.17), I address effects of the parallel component of the 3D

field $\mathbf{b}_0 \cdot \delta\mathbf{B}$ and of the magnetic surface deformation $\boldsymbol{\xi} \cdot \boldsymbol{\nabla} B_0$ on zonal flows in this work. Contribution from the perpendicular component of the 3D field is of order δ^2, and is thus neglected in Eq. (4.17). We use following model for the Lagrangian variation of the magnetic field strength.

$$\delta_{\mathrm{L}} B(\mathbf{x}_0) = B_0 \sum_m \delta_m \cos\left[m\theta - n\zeta + \chi_m\right], \tag{4.18}$$

where m and n are poloidal and toroidal mode number of the static 3D field, respectively. χ_m is the phase constant of the mth component of the 3D field. Here we assume m and n to be $\mathcal{O}(1)$. This assumption with a subsidiary ordering of $\delta \ll \epsilon$ assures the negligible effects from the helicity induced magnetic trapping [141]. The resulting expression of the magnetic field strength is

$$B(\mathbf{x}) \simeq B_0 \left[1 - \epsilon\cos\theta + \sum_m \delta_m \cos\left[(m - nq)\theta - n\alpha + \chi_m\right]\right], \tag{4.19}$$

where $\alpha = \zeta - q\theta$ is an angle-like field line label. Note that r, θ, ζ (and thus α) are magnetic coordinates defined on the basis of the undeformed magnetic surface.

As a next step, I perform an explicit calculation of the orbit-averaged radial magnetic drift, which is the origin of the phase mixing in velocity space. General expression of the 3D field induced slow radial drift in high aspect ratio tokamak is as follows.

$$\overline{v}_{\mathrm{D}\psi} = \overline{\mathbf{v}}_{\mathrm{D}} \cdot \boldsymbol{\nabla}\psi = \frac{1}{\tau_{\mathrm{b/t}}} \frac{\partial J_{\mathrm{b/t}}}{\partial \alpha} \simeq -\frac{1}{e} \overline{\left(\mu \frac{\partial B}{\partial \alpha}\right)}. \tag{4.20}$$

Here $\tau_{\mathrm{b/t}}$ and $J_{\mathrm{b/t}}$ are period and adiabatic invariant of bounce/transit motion, respectively. $\overline{A} \equiv \oint (dlA/v_\parallel) / \oint (dl/v_\parallel)$ is the bounce/transit orbit average, and is calculated with its lowest order expression, i.e., with $dl \simeq qRd\theta$ and $v_\parallel \simeq \sqrt{(2/M)[E - \mu B_0(1 - \epsilon\cos\theta)]}$. Substitution of Eq. (4.19) into Eq. (4.20) yields

the general expression of $\overline{\omega}_{\rm D} = \overline{v}_{{\rm D}\psi} S'(\psi)$:

$$\overline{\omega}_{\rm D} = \begin{cases} -\dfrac{k_r \rho_{\rm th}}{R}\sqrt{\dfrac{E}{T}}\sqrt{\dfrac{\mu B_0}{M}} \displaystyle\sum_m \frac{\delta_m}{\epsilon} \frac{nq}{2K(\kappa)} \sin\left(n\alpha + \chi_m\right) \\ \qquad\qquad \times \displaystyle\int_0^{\theta_b} d\theta \, \frac{\cos\left[(m-nq)\theta\right]}{\sqrt{\kappa^2 - \sin^2\left(\theta/2\right)}} & \text{Ⓣ} \\ -\dfrac{k_r \rho_{\rm th}}{R}\sqrt{\dfrac{E}{T}}\sqrt{\dfrac{\mu B_0}{M}} \displaystyle\sum_m \frac{\delta_m}{\epsilon} \frac{nq\kappa}{2K(\kappa^{-1})} \sin\left(n\alpha + \chi_m\right) \\ \qquad\qquad \times \displaystyle\int_0^{\pi} d\theta \, \frac{\cos\left[(m-nq)\theta\right]}{\sqrt{\kappa^2 - \sin^2\left(\theta/2\right)}} & \text{Ⓟ} \end{cases} \tag{4.21}$$

where $\rho_{\rm th} = v_{\rm th}/\Omega$ is the thermal gyroradius, $v_{\rm th} = \sqrt{T/M}$ is the thermal speed and θ_b is the poloidal angle at turning point. The pitch angle parameter κ is defined by

$$\kappa^2 \equiv \frac{E - \mu B_0(1-\epsilon)}{2\epsilon\mu B_0}, \tag{4.22}$$

and Ⓣ and Ⓟ denote trapped ($\kappa < 1$) and passing ($\kappa > 1$) particles, respectively. At this point I assume deeply-trapped and strongly-passing particles in my explicit calculation of the orbit-averaged radial drift frequency $\overline{\omega}_{\rm D}$. Then, Eq. (4.21) is simplified as

$$\overline{\omega}_{\rm D} = \begin{cases} -nq\dfrac{k_r \rho_{\rm th}}{R}\sqrt{\dfrac{E}{T}}\sqrt{\dfrac{\mu B_0}{M}} \displaystyle\sum_m \frac{\delta_m}{\epsilon} \sin\left(n\alpha + \chi_m\right) & \text{Ⓣ} \\ -nq\dfrac{k_r \rho_{\rm th}}{R}\sqrt{\dfrac{E}{T}}\sqrt{\dfrac{\mu B_0}{M}} \dfrac{\delta_{m_0}}{\epsilon} \sin\left(n\alpha + \chi_{m_0}\right) & \text{Ⓟ} \end{cases} \tag{4.23}$$

where $m_0 = nq$ corresponds to the index of the 3D field component resonant to the $q(r) = m_0/n$ rational surface. Details of the calculation are presented in Appendix. Disappearance of the non-resonant components in Eq. (4.23) for passing particles is a result of the strongly-passing particle approximation. In reality, the non-resonant components of the 3D field would give a small, yet not vanishing contribution to the orbit-averaged radial drift of passing particles. In Eq. (4.23), the orbit-averaged radial drift is indeed energy dependent, and this

property leads to the phase-mixing in velocity space. The radial drift frequency $\overline{\omega}_{\rm D}$ can be written in a different form by introducing δ_t and χ_t which contain multi m-component effect on the orbit-averaged radial drift:

$$\overline{\omega}_{\rm D} = \begin{cases} -nq\dfrac{k_r\rho_{\rm th}}{R}\sqrt{\dfrac{E}{T}}\sqrt{\dfrac{\mu B_0}{M}}\dfrac{\delta_t}{\epsilon}\sin(n\alpha+\chi_t) & \text{Ⓣ} \\ -nq\dfrac{k_r\rho_{\rm th}}{R}\sqrt{\dfrac{E}{T}}\sqrt{\dfrac{\mu B_0}{M}}\dfrac{\delta_{m_0}}{\epsilon}\sin\left(n\alpha+\chi_{m_0}\right) & \text{Ⓟ} \end{cases} \tag{4.24}$$

where

$$\delta_t \equiv \Big[\big(\sum_m \delta_m\cos\chi_m\big)^2 + \big(\sum_m \delta_m\sin\chi_m\big)^2\Big]^{1/2} \tag{4.25}$$

and

$$\chi_t \equiv \tan^{-1}\left(\frac{\sum_m \delta_m\sin\chi_m}{\sum_m \delta_m\cos\chi_m}\right). \tag{4.26}$$

Here the effective amplitude δ_t and the effective phase χ_t characterize the multi-m effect of the RMP on trapped particles. Note that $\overline{\omega}_{\rm D}$ is independent of the pitch-angle parameter κ under the assumptions of deeply-trapped and strongly-passing particles.

4.2.1 Long wavelength regime

I now present explicit calculation of $\langle I(t)\rangle$ and $\mathcal{D}(t)$ in various wavelength regimes. In the long-wavelength limit $k_r\rho_i \ll 1$, following Ref. [140]. From Eq. (4.13) and Eq. (4.15), the expressions of $\langle I(t)\rangle$ and $\mathcal{D}(t)$ are

$$\langle I(t)\rangle \simeq k_r^2\rho_{{\rm th}i}^2\frac{e\phi_{\rm k}(0)}{T_i}\left\langle\int d^3v F_{i0}e^{-i\overline{\omega}_{{\rm D}i}t}\right\rangle, \tag{4.27}$$

and

$$\begin{aligned}\mathcal{D}(t) \simeq &\left\langle\int d^3v F_{i0}\left[1-(1-k_r^2\rho_i^2/2+\overline{Q_i}^2-\overline{Q_i^2})e^{-i\overline{\omega}_{{\rm D}i}t}\right]\right\rangle \\ &+\frac{T_i}{T_e}\left\langle\int d^3v F_{e0}\left[1-e^{-i\overline{\omega}_{{\rm D}e}t}\right]\right\rangle,\end{aligned} \tag{4.28}$$

in the long wavelength limit. Note that the flux-surface average is $\langle\cdots\rangle \simeq (2\pi)^{-2}\oint d\theta \oint d\zeta(\cdots)$. Since the dependence on the magnetic field line label α (or, on the toroidal angle ζ equivalently) exists only in $\overline{\omega}_{\rm D}$,

$$\left\langle [\cdots] e^{-i\overline{\omega}_{\rm D} t} \right\rangle \simeq \begin{cases} \langle [\cdots] J_0(\gamma_t t E/T)\rangle_\theta & \text{Ⓣ} \\ \langle [\cdots] J_0(\gamma_0 t E/T)\rangle_\theta & \text{Ⓟ} \end{cases} \tag{4.29}$$

with high aspect ratio approximation. Here, $\langle\cdots\rangle_\theta \equiv (2\pi)^{-1}\oint d\theta(\cdots)$, and

$$\gamma_t = nq\, k_r \rho_{\rm th} \frac{v_{\rm th}}{R}\frac{\delta_t}{\epsilon}, \qquad \gamma_0 = nq\, k_r \rho_{\rm th} \frac{v_{\rm th}}{R}\frac{\delta_{m_0}}{\epsilon}. \tag{4.30}$$

The following integration formula [156] is useful to calculate the velocity integrations.

$$\int_0^\infty dx\, e^{-ax} J_\nu(bx) x^{\mu-1} = (a^2+b^2)^{-\mu/2}\Gamma(\nu+\mu) P_{\mu-1}^{-\nu}[a(a^2+b^2)^{-1/2}], \tag{4.31}$$

for $a > 0$, $b > 0$ and $\mathrm{Re}(\nu+\mu) > 0$. Here $P_\lambda^\mu(x)$ is the Legendre function. Consequent expression of $\langle I(t)\rangle$ and $\mathcal{D}(t)$ are

$$\langle I(t)\rangle = n_0 k_r^2 \rho_{{\rm th}i}^2 \frac{e\phi_{\rm k}(0)}{T_i}\frac{1}{[1+(\gamma_{0i}t)^2]^{1/2}}, \tag{4.32}$$

and

$$\begin{aligned}\mathcal{D}(t) = n_0 \Bigg[& 1 - \frac{1}{[1+(\gamma_{0i}t)^2]^{1/2}} + k_r^2\rho_{{\rm th}i}^2 \Bigg\{ \frac{1}{[1+(\gamma_{0i}t)^2]^{3/2}} \\ & + 1.20\frac{q^2}{\epsilon^{1/2}}\frac{P_{3/2}([1+(\gamma_{ti}t)^2]^{-1/2})}{[1+(\gamma_{ti}t)^2]^{5/4}} + 0.43\frac{q^2}{\epsilon^{1/2}}\frac{P_{3/2}([1+(\gamma_{0i}t)^2]^{-1/2})}{[1+(\gamma_{0i}t)^2]^{5/4}} \Bigg\} \\ & + \frac{T_i}{T_e}\left\{ 1 - \frac{1}{[1+(\gamma_{0e}t)^2]^{1/2}} \right\} \Bigg]. \end{aligned} \tag{4.33}$$

Note that the third term comes from the finite Larmor radius (FLR) of ions, and the fourth and the fifth terms come from the FOW of the trapped and the passing ions, respectively. Note that for FLR and FOW effects we did not

assume deeply trapped and strongly passing approximations. As a consequence, we obtain an asymptotic form of the zonal flow response function in long-wavelength limit,

$$\frac{\phi_{\rm k}(t)}{\phi_{\rm k}(0)} \approx \begin{cases} \dfrac{1}{1+1.6q^2/\epsilon^{1/2}} & \text{for } \gamma_{0i,e}^{-1} > t \gg \omega_{{\rm b}i}^{-1} \\ \dfrac{k_r^2\rho_{{\rm th}i}^2}{(1+T_i/T_e)\gamma_{0i}t} & \text{for } t > \gamma_{0i,e}^{-1} \end{cases} . \tag{4.34}$$

We recover the Rosenbluth-Hinton residual zonal flow level [140] in the short-time limit of $\phi_{\rm k}(t)/\phi_{\rm k}(0)$. In the long-time limit, an algebraic decay of $\phi_{\rm k}(t)/\phi_{\rm k}(0)$ occurs due to the phase-mixing of the zonal mode distribution function. Note that the expressions of decay for the FOW terms and those for other terms are different due to different contributions of strongly passing particles ($\kappa^2\epsilon > 1$). For FOW terms their contribution is negligibly small, while it is not for other terms. It is also worth noting that the contribution from trapped particles is comparable with that from passing particles for FOW terms, while it is negligible for other terms. The long-time asymptotic behavior in Eq. (4.34) does not change even if we consider effects of the higher order terms in $k_r\rho_i$ in the long wavelength regime $k_r\rho_i < Q_i < 1$. The higher order terms may change the form of $\mathcal{D}(t)$, but their effects become unimportant as time increases since they lead to faster decay. The only change in the long time behavior is $k_r^2\rho_{{\rm th}i}^2 \to (1-\Gamma_0)/\Gamma_0$ in $\langle I(t)\rangle$, as we apply the general expression of the ion polarization density.

4.2.2 Intermediate and short wavelength regimes

For the intermediate wavelength regime $k_r\rho_i < 1 < Q_i$ and the short wavelength regime $1 < k_r\rho_i < Q_i$, we can calculate $\langle I(t)\rangle$ and $\mathcal{D}(t)$ explicitly with deeply-trapped and strongly-passing approximations, by consulting Refs. [82,157]. For

the intermediate wavelength regime, we neglect the FLR effects and use the large argument asymptotic form of the Bessel functions for the bounce averaging as

$$\overline{e^{iQ}} \simeq J_0(a\kappa) \simeq \sqrt{\frac{2}{\pi a\kappa}} \cos\Big(a\kappa - \frac{\pi}{4}\Big), \tag{4.35}$$

and the stationary phase approximation for the transit averaging as

$$\overline{e^{iQ}} \simeq \sqrt{\frac{2\kappa}{\pi a}} \exp\Big[i\Big(a\kappa - \frac{\pi}{4}\Big)\Big]. \tag{4.36}$$

Here $a = 2\sqrt{\epsilon} k_r \rho_{\theta \mathrm{th}} \sqrt{E/T}$, and $\rho_{\theta \mathrm{th}} = (q/\epsilon)\rho_{\mathrm{th}}$ is the thermal poloidal gyroradius. Substituting Eqs. (4.24), (4.35) and (4.36) into Eqs. (4.13) and (4.15), we obtain expressions of $\langle I(t)\rangle$ and $\mathcal{D}(t)$ in the intermediate regime

$$\langle I(t)\rangle = n_0 \frac{1-\Gamma_0}{\Gamma_0} \frac{e\phi_{\mathrm{k}}(0)}{T_i} \frac{1}{2^{1/2}\pi^{3/2}} \frac{1}{k_r q \rho_{\mathrm{th}i}} \frac{1}{[1+(\gamma_{0i}t)^2]^{1/2}}, \tag{4.37}$$

$$\begin{aligned}\mathcal{D}(t) =& n_0 \left[1 - \frac{1}{\sqrt{2\epsilon}}\left(1 - \frac{\sqrt{2\epsilon}}{2}\right) \frac{1}{\pi^{3/2}} \frac{1}{k_r \rho_{\theta \mathrm{th}i}} \frac{1}{[1+(\gamma_{0i}t)^2]^{1/2}}\right. \\ &\left. + \sqrt{2\epsilon} \frac{1}{\pi^{3/2}} \frac{1}{k_r \rho_{\theta \mathrm{th}i}} \frac{1}{[1+(\gamma_{ti}t)^2]^{1/2}} + \frac{T_i}{T_e}\left\{1 - \frac{1}{[1+(\gamma_{0e}t)^2]^{1/2}}\right\}\right]. \end{aligned} \tag{4.38}$$

For the short wavelength regime, we use the asymptotic form of the Bessel functions for the FLR effect as

$$J_0(k_r\rho) \simeq \sqrt{\frac{2}{\pi k_r \rho}} \cos\Big(k_r\rho - \frac{\pi}{4}\Big), \tag{4.39}$$

with approximate forms Eqs. (4.35) and (4.36) for the FOW effects. Consequent expressions of $\langle I(t)\rangle$ and $\mathcal{D}(t)$ are

$$\langle I(t)\rangle = n_0 \frac{1-\Gamma_0}{\Gamma_0} \frac{e\phi_{\mathrm{k}}(0)}{T_i} \frac{\Gamma(1/4)}{2\pi^{5/2}} \frac{1}{k_r q \rho_{\mathrm{th}i}} \frac{1}{k_r \rho_{\mathrm{th}i}} \frac{P_{-1/2}([1+(\gamma_{0i}t)^2]^{-1/2})}{[1+(\gamma_{0i}t)^2]^{1/4}}, \tag{4.40}$$

$$\begin{aligned}\mathcal{D}(t) = n_0 & \left[1 - \frac{1}{\sqrt{2\epsilon}}\left(1 - \frac{\sqrt{2\epsilon}}{2}\right) \frac{\Gamma(1/4)}{2^{1/2}\pi^{5/2}} \frac{1}{k_r \rho_{\theta \mathrm{th}i}} \frac{1}{k_r \rho_{\mathrm{th}i}} \frac{P_{-1/2}([1+(\gamma_{0i}t)^2]^{-1/2})}{[1+(\gamma_{0i}t)^2]^{1/4}}\right. \\ &+ \sqrt{2\epsilon} \frac{\Gamma(1/4)}{2^{1/2}\pi^{5/2}} \frac{1}{k_r \rho_{\theta \mathrm{th}i}} \frac{1}{k_r \rho_{\mathrm{th}i}} \frac{P_{-1/2}([1+(\gamma_{ti}t)^2]^{-1/2})}{[1+(\gamma_{ti}t)^2]^{1/4}} \\ &\left. + \frac{T_i}{T_e}\left\{1 - \frac{1}{[1+(\gamma_{0e}t)^2]^{1/2}}\right\}\right]. \end{aligned} \tag{4.41}$$

We note that for the neoclassically enhanced polarization shielding $\mathcal{D}(t)$, the contribution from trapped particles is smaller than that from passing particles by an order of ϵ, in both intermediate and short wavelength regimes. Now it is obvious that the contribution from trapped particles on the zonal flow response is non-negligible only in the long wavelength regime. Finally, we summarize the long-time ($t > \gamma_{0i.e}^{-1}$) asymptotic behavior of the zonal flow response to the leading order in ϵ as follows.

$$\frac{\phi_{\mathbf{k}}(t)}{\phi_{\mathbf{k}}(0)} \approx \begin{cases} \dfrac{1-\Gamma_0}{\Gamma_0}\dfrac{1}{(1+T_i/T_e)\gamma_{0i}t} & (k_r\rho_i < Q_i < 1) \\ \dfrac{1}{2^{1/2}\pi^{3/2}}\dfrac{1}{k_r q\rho_{\mathrm{th}i}}\dfrac{1-\Gamma_0}{\Gamma_0}\dfrac{1}{(1+T_i/T_e)\gamma_{0i}t} & (k_r\rho_i < 1 < Q_i) \\ \dfrac{\Gamma(1/4)}{2\pi^{5/2}}\dfrac{1}{k_r q\rho_{\mathrm{th}i}}\dfrac{1}{k_r\rho_{\mathrm{th}i}}\dfrac{1-\Gamma_0}{\Gamma_0}\dfrac{P_{-1/2}(1/\gamma_{0i}t)}{(1+T_i/T_e)(\gamma_{0i}t)^{1/2}} & (1 < k_r\rho_i < Q_i) \end{cases} . \tag{4.42}$$

This equation shows a time-asymptotic algebraic decay of residual zonal flow. Note that for the RMP field case, the influence of the resonant component is dominant in the 3D field induced zonal flow decay. The long-time collisionless decay occurs mainly due to the orbit-averaged radial drift and consequent phase-mixing of passing particles. In Fig. 4.1, we compare long-time evolution of the residual zonal flows of different wavelength regimes, using the expressions of $\langle I(t)\rangle$ and $\mathcal{D}(t)$ previously obtained. Note that the normalization factor γ in the figure is defined not to contain the wavelength dependency, while the characteristic phase-mixing rate γ_{0i} is proportional to $k_r\rho$. Fig. 4.1 reveals that shorter wavelength zonal flows undergo faster decay.

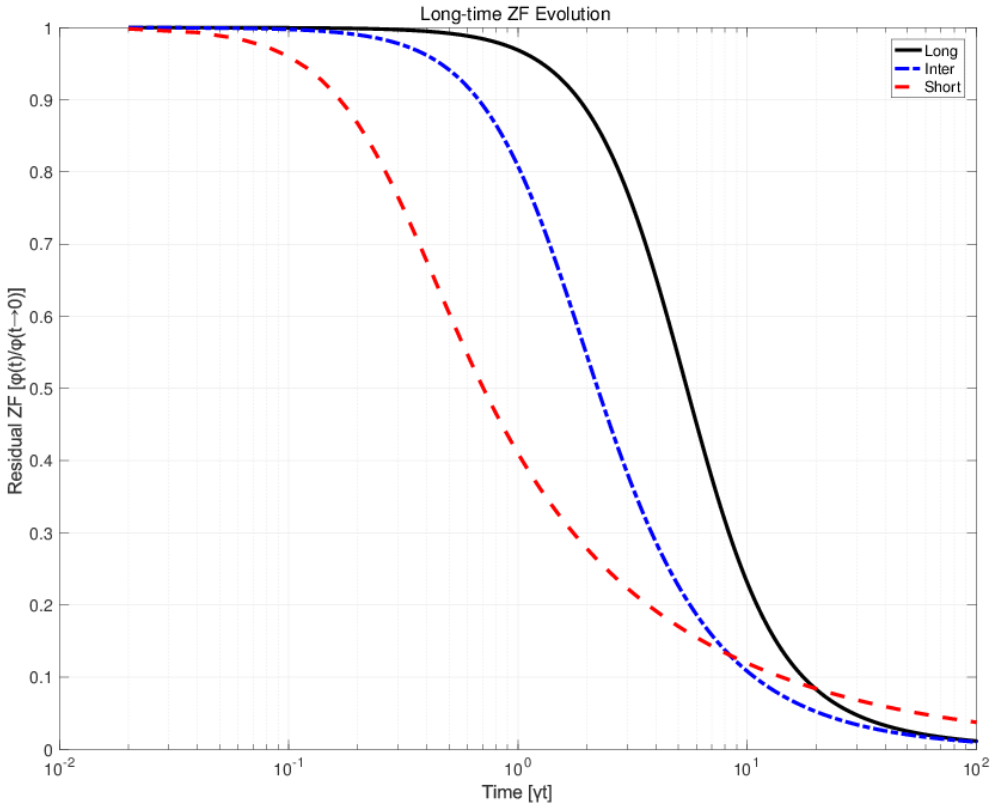

Figure 4.1 Long time evolution of the residual zonal flow level as a function of a normalized time γt for $k_r \rho_{\mathrm{th}i} = 0.1$ (solid black), 0.5 (dash-dot blue) and 2.5 (dashed red). The normalization factor is $\gamma = nq(v_{\mathrm{th}i}/R)(\delta/\epsilon)$, where $\delta = \delta_{m_0} = \delta_t$ is assumed for an estimation. We choose $q = 6$, $\epsilon = 0.25$ and $T_i/T_e = 1$ as a reference set.

4.3 Discussion on experimental applications

In the previous sections, I identified that the single-n (but multi-m) RMP field induces time-asymptotic algebraic zonal flow decay as a consequence of the velocity space phase-mixing due to energy-dependent radial drifts. To address its relevance in practical situations, one should compare this long-time collisionless decay with the collisional zonal flow damping using typical tokamak parameters. Following Ref. [151], we use an expression $\gamma_{\rm coll} = \nu_{ii}/1.5\epsilon$ for the collisional damping rate. Here ν_{ii} is the ion-ion collision frequency [158]. I obtained the characteristic frequency of the RMP induced decay in the previous section as $\gamma_{\rm 3D} = \gamma_{0i} = nqk_r\rho_{{\rm th}i}(v_{{\rm th}i}/R)(\delta_{m_0}/\epsilon)$. For an estimation, we use parameters of KSTAR L-mode plasma just prior to L-H transition near the position of H-mode pedestal top [131,159,160]. These are $q = 6$, $R = 2.25$ m, $n_e = 0.5 \times 10^{19}$ m^{-3} and $T_i = 0.5$ keV, together with parameters of a typical KSTAR RMP field $n = 1$ and $\delta = 10^{-3}$ [148]. Then, the ratio of the RMP induced zonal flow decay rate to the collisional zonal flow damping rate becomes

$$\gamma_{\rm 3D}/\gamma_{\rm coll} \sim 2.5k_r\rho_{{\rm th}i}. \tag{4.43}$$

This indicates that the RMP induced zonal flow decay can play a dominant role compared to the collisional zonal flow damping for intermediate and short wavelength zonal flows. For this simple comparison, the following caveats should be kept in mind. The collisionless decay in Eq. (4.42) is algebraic in time. So the actual decay is slower than the exponential decay with the rate $\gamma_{\rm 3D}$. On the other hand, the collisional decay in Eq. (29) of Ref. [151] has a complicated time-dependence which is not a simple exponential decay. Nevertheless, gyrokinetic simulation result in Ref. [161] indicates that $\gamma_{\rm coll} = \nu_{ii}/1.5\epsilon$ can be taken as the effective damping rate of zonal flow. Also note that the zonal potential

asymptotes to a very small, but non-zero value. So in this sense, we are slightly overestimating both the collisionless and collisional decrease of zonal flows in time. More quantitative comparison could be possible using a time-integrated value [151] of the zonal potential as done in Ref. [162]. For this, some modification is probably required to avoid possible divergence of integrals.

Of course, an extension of gyrokinetic simulation of Ref. [161] is desirable to assess the importance of the mechanism proposed in this work. It is note-worthy that simulations in Ref. [146] indicate no significant difference in electrostatic turbulence level or zonal flow intensity for different amplitudes of RMP fields for DIII-D plasma parameters during H-mode phase. The 3D equilibrium used in those simulations presumably contains the parallel component of magnetic perturbation. It remains to be seen if the conclusion changes if simulations are performed for parameters just prior to the L-H transition in which zonal flows are expected to play more prominent roles [4, 138, 139].

Nonlinear gyrokinetic simulations [163, 164] and experimental observations [37] have indicated that significant level of intermediate and short wavelength zonal flows can exist in tokamak plasmas. Therefore, the RMP induced collisionless zonal flow decay should be considered as an important piece of the zonal flow dynamics in the L-H transition. It is worth noting that the RMP induced collisionless zonal flow decay rate ($\propto T_i$) increases with temperature while the collisional zonal flow damping rate ($\propto T_i^{-3/2}$) decreases. Therefore, I expect prominent role of the RMP induced zonal flow decay in future tokamaks including ITER [165].

As zonal flows may play a key role in triggering the L-H transition by regulating tokamak turublence [4], my result indicates that stronger RMP field will lead to lower zonal flow level and thus higher L-H transition power threshold.

Note that my theory considers a composite 3D field effect on the magnetic field strength variation and on the zonal flow response. From Eq. (4.17), it is obvious that the parallel (to the tokamak magnetic field) component of the 3D field $\delta B_{\parallel}$ contributes to the phase-mixing and the collisionless decay, and the radial component δB_r enters indirectly through the magnetic surface deformation term. Recent experimental results from KSTAR [166] show that the threshold increase is more significant with $n = 2$ RMP compared to the case with $n = 1$ RMP at the same field amplitude. This n-dependence of the transition power threshold agrees with the trend predicted from my result (Eq. (4.30)). The characteristic frequency of the 3D field induced phase-mixing and zonal flow decay is proportional to n. My theory suggests stronger zonal flow decay and thus higher L-H transition power threshold with higher-n RMP at the same field amplitude.

Measurement of radial wavenumber spectrum of zonal flow for instance via phase contrast imaging (PCI) [167] or heavy ion beam probe (HIBP) [168, 169] enables us to validate effectiveness of my theory. My theory predicts stronger RMP induced zonal flow decay for higher-k_r zonal flows, while others predict weaker damping for higher-k_r [145] or no k_r-dependence [143, 144]. I expect lower proportion of intermediate and short wavelength zonal flows in k_r spectrum for stronger RMP amplitude. Therefore, observations of k_r spectra from experiments with different RMP amplitudes will clearly reveal effectiveness of my theory. Note that it is desirable to keep edge safety factor profile the same in the series of experiments, because positions of rational surfaces, which is deeply connected with the issue of RMP field penetration, is sensitive to the edge safety factor profile.

More recent KSTAR experiments [170] reveal that non-resonant magnetic perturbations (NRMPs), unlike RMPs, do not have significant influence on L-H

transition power threshold. These results indicate that resonant component of 3D field plays an important role. Recall that in my theory of RMP induced collisionless zonal flow decay, resonant component of the applied 3D field is a main player and effects from non-resonant components are subdominant. Again, my theory and experimental results agree in trend. Note, however, that there are other routes for RMP to affect turbulence suppression and H-mode transition threshold. Enhanced transport in RMP-induced stochastic magnetic field region can change various profiles. Also, RMP can make toroidal J×B torque by non-ideal MHD response [171], which results in change of toroidal rotation profile. Consequently, radial electric field and thus E×B shear profiles change through radial force balance. While both mesoscale zonal E×B flows and macroscale E×B flows play important roles in H-mode transition, their relative importance in determining transition criterion can be different depending on the situation.

Chapter 5

Conclusion

In this thesis, I presented three theoretical extensions of E×B shear suppression using gyrokinetics, bounce-kinetics and two-point renormalization to explain detailed issues of turbulence suppression and transport barrier formation. I extended two-point theory of E×B shear suppression to consider tilted turbulence eddies which are frequently observed in simulations and experiments. I obtained and analysed a generalized criterion of E×B shear suppression. Revealed dependence of efficiency of turbulence suppression on the sign of E×B shear was applied to explain up-down asymmetry of H-mode transition power threshold in single-null diverted plasmas. For trapped electron turbulence, I showed that radial shear of magnetic precession of trapped electrons play an important role together with E×B flow shear in turbulence suppression toward formation of electron thermal ITB. For that purpose, a systematic derivation of a proper two-point equation from modern bounce-kinetic formalism was performed. It was naturally revealed that synergism between trapped electron pre-

cession shear and E×B shear depends on their relative sign, and that magnetic shear interplay with them to nonlinearly suppress trapped electron turbulence and form electron thermal ITB. I also performed a theoretical analysis of RMP effect on tokamak zonal flows using gyrokinetc equations. I extended previous theoretical works of zonal flow evolution in tokamaks and stellarators, and found that RMP induced secular radial magnetic drifts induce long-term collisionless decay of zonal flows. This is a natural extension of previously studied collisionless damping due to radial magnetic drifts in tokamak and stellarator magnetic fields. My theory provides an explanation of increase of H-mode transition power threshold with RMP amplitude. Parameter dependence of the rate of RMP induced zonal flow decay shows that it can play a significant role in present day tokamaks, and may be dominant in future machines. Dependence of the RMP induced decay on toroidal mode number of RMP is a unique feature of my theory, and it agree with recent KSTAR experimental results.

As a closing remark, I make a short comment on recent trend of theoretical study of E×B flow effect on fusion turbulence. Radial mesoscale dynamics has been topics of growing interest in magnetic fusion turbulence theory community, and various routes of interactions between E×B flows and turbulence have been investigated during last two decades. For macroscale E×B shear flows, their influence on turbulence spreading has been explored using analytic model studies, followed by demonstration via gyrokinetic simulations and experimental applications. Similar collaboration of model studies and gyrokinetic simulations has been done to explore reduction of avalanches by macroscale E×B flows, which appears as decrease of long-tail in non-Gaussian probability distribution function of fluxes. For mesoscale zonal flows, interactions of zonal flows and turbulence, traditionally interpreted using local 0D predator-prey models, have been extended to 1D to include robust radial dynamics. A

recently highlighted topic is formation of E×B staircase, which is an alternative quasi-periodic radial pattern of E×B shear layer and avalanching region. However, theoretical studies of mesoscale dynamics of E×B shear flows have been mostly limited to reduced fluid models of wave turbulence. Generalization of analytic theories using gyrokinetic equations should be performed. Especially, neoclassical effects on physics of E×B shear reduction of turbulence should be investigated and identified to understand realistic fusion plasmas, toward quantitative agreement with experiments. Finally, we have to aim to reach thorough understanding of synergistic effects of macroscale E×B flows and zonal flows, for a complete theoretical prediction of transport barrier formation. Roles of non-wave-like turbulence eddies on aforementioned issues should also be investigated for mature understanding of fusion turbulence. I hope contents in this thesis will be used as a reference for these future theory development.

Appendix A

Explicit calculation of secular magnetic drift frequency

In this Appendix, I present an explicit calculation of the secular radial magnetic drift frequency $\overline{\omega}_{\rm D}$ near a rational surface, in the presence of RMP field which yields an approximate expression in Eq. (4.23). I start from Eq. (4.21). Following Ref. [172], I Taylor-expand the safety factor q as $q(r) = q(r_s)+x/\Delta+\cdots$, where r_s is radial position of a rational surface, $x \equiv r - r_s$ is the displacement from the rational surface, and $\Delta \equiv 1/(nq')$ is radial distance between two nearby rational surfaces. Here $q' = dq(r)/dr$. Note that $q(r_s) = m_0/n$ where m_0 is the index of the resonant component of the RMP induced magnetic field strength variation. Then, with $p \equiv m - m_0$ and applying deeply-trapped ($\kappa \ll 1$) and strongly-passing ($\kappa \gg 1$) approximation, I calculate the last factor $\int d\theta(\cdots)$ in

Eq. (4.21) which result in the following expression.

$$\overline{\omega}_{\mathrm{D}} \approx \begin{cases} -nq\dfrac{k_r\rho_{\mathrm{th}}}{R}\sqrt{\dfrac{E}{T}}\sqrt{\dfrac{\mu B_0}{M}}\displaystyle\sum_p \dfrac{\delta_{p+m_0}}{\epsilon}\sin\left(n\alpha+\chi_{p+m_0}\right) & \\ \qquad\qquad \times J_0[2\kappa(x-p\Delta)/\Delta] & \text{Ⓣ} \\ -nq\dfrac{k_r\rho_{\mathrm{th}}}{R}\sqrt{\dfrac{E}{T}}\sqrt{\dfrac{\mu B_0}{M}}\displaystyle\sum_p \dfrac{\delta_{p+m_0}}{\epsilon}\sin\left(n\alpha+\chi_{p+m_0}\right) & \\ \qquad\qquad \times \dfrac{\sin\left[\pi(p-x/\Delta)\right]}{\pi(p-x/\Delta)} & \text{Ⓟ} \end{cases} \tag{A.1}$$

Here, I used $K(\kappa) \approx \pi/2$, $\theta \approx \sin\theta$ for trapped particles [172], and $K(\kappa^{-1}) \approx \pi/2$ for passing particles. Since I am calculating $\overline{\omega}_{\mathrm{D}}$ near a rational surface, x/Δ is considered to be small, i.e., $x/\Delta \ll 1$ and thus Eq. (A.1) can be further approximated as follows.

$$\overline{\omega}_{\mathrm{D}} \approx \begin{cases} -nq\dfrac{k_r\rho_{\mathrm{th}}}{R}\sqrt{\dfrac{E}{T}}\sqrt{\dfrac{\mu B_0}{M}}\displaystyle\sum_p \dfrac{\delta_{p+m_0}}{\epsilon}\sin\left(n\alpha+\chi_{p+m_0}\right)J_0(2\kappa p) & \text{Ⓣ} \\ -nq\dfrac{k_r\rho_{\mathrm{th}}}{R}\sqrt{\dfrac{E}{T}}\sqrt{\dfrac{\mu B_0}{M}}\dfrac{\delta_{m_0}}{\epsilon}\sin\left(n\alpha+\chi_{m_0}\right) & \text{Ⓟ} \end{cases} \tag{A.2}$$

For a simple expression I use $J_0(2\kappa p) \approx 1$ for trapped particles, as an ensuing result of the deeply-trapped approximation. Finally, I obtain the expression Eq. (4.23).

Bibliography

[1] K.H. Burrell, Phys. Plasmas **4**, 1499 (1997)

[2] P.W. Terry, Rev. Mod. Phys. **72**, 109 (2000)

[3] T.S. Hahm, Plasma Phys. Control. Fusion **44**, A87 (2002)

[4] P.H. Diamond *et al.*, Plasma Phys. Control. Fusion **47**, R35 (2005)

[5] K. Itoh *et al.*, Phys. Plasmas **13**, 055502 (2006)

[6] T.H. Dupree, Phys. Fluids **15**, 334 (1972)

[7] P.W. Terry and P.H. Diamond, Phys. Fluids **28**, 1419 (1985)

[8] H. Biglari, P.H. Diamond and P.W. Terry, Phys. Fluids B **2**, 1 (1990)

[9] Y. Kosuga *et al.*, Phys. Plasmas **21**, 102303 (2014)

[10] T.S. Hahm, Phys. Plasmas, **1**, 2940 (1994)

[11] T.S. Hahm and K.H. Burrell, Phys. Plasmas **2**, 1648 (1995)

[12] T.S. Hahm, Phys. Plasmas **4**, 4074 (1997)

[13] W. Horton, R.D. Estes and D. Biskamp, Plasma Phys. **22**, 663 (1980)

[14] W. Horton, D.-I. Choi and W.M. Tang, Phys. Fluids **24**, 1077 (1981)

[15] G.S. Lee and P.H. Diamond, Phys. Fluids **29**, 3291 (1986)

[16] J.W. Connor, Nucl. Fusion **26**, 193 (1986)

[17] W.W. Lee and T.M. Tang, Phys. Fluids **31**, 612 (1988)

[18] T.S. Hahm and T.M. Tang, Phys. Plasmas **3**, 242 (1996)

[19] T.H. Dupree and D.J. Tetreault, Phys. Fluids **21**, 425 (1978)

[20] T.H. Dupree, Phys. Fluids **9**, 1773 (1966)

[21] T.H. Dupree, Phys. Fluids **10**, 1049 (1967)

[22] P.H. Diamond, S.-I. Itoh and K. Itoh, *Modern Plasma Physics Volume 1*, Cambridge University Press (2010)

[23] H. Biglari, P.H. Diamond and P.W. Terry, Phys. Fluids **31**, 2644 (1988)

[24] J.W. Conner, R.J. Hastie and J.B. Taylor, Proc. Royal Soc. A **365**, 1 (1979)

[25] E.A. Frieman and Liu Chen, Phys. Fluids **25**, 502 (1982)

[26] T.M. Antonsen Jr. *et al.*, Phys. Plasmas **3**, 2221 (1996)

[27] M. Yoshida *et al.*, Nucl. Fusion **55**, 073014 (2015)

[28] N. Fedorczak *et al.*, Nucl. Fusion **52**, 103013 (2012)

[29] F. Wagner, Plasma Phys. Control. Fusion **49**, B1 (2007)

[30] L. Schmitz *et al.*, Phys. Rev. Lett. **108**, 155002 (2012)

[31] G.R. McKee *et al.*, Nucl. Fusion **49**, 115016 (2009)

[32] M.W. Shafer *et al.*, Phys. Plasmas **19**, 032504 (2012)

[33] I.U. Uzun-Kaymak, R.J. Fonck and G.R. McKee, Rev. Sci. Instrum. **83**, 10D526 (2012)

[34] E. Viezzer *et al.*, Rev. Sci. Instrum. **83**, 103501 (2012)

[35] B.W. Rice *et al.*, Rev. Sci. Instrum. **70**, 815 (1999)

[36] N.C. Hawkes *et al.*, Rev. Sci. Instrum. **70**, 894 (1999)

[37] J.C. Hillesheim *et al.*, Phys. Rev. Lett. **116**, 065002 (2016)

[38] I. Shesterikov *et al.*, Phys. Rev. Lett. **111**, 055006 (2013)

[39] I. Cziegler *et al.* Nucl. Fusion **55**, 083007 (2015)

[40] F. Clairet *et al.*, presented at *the 45th EPS Conference on Plasma Physics* (Prague, Czech Republic, 2018)

[41] P. Hennequin *et al.*, presented at*the 2nd Asia-Pacific Conference on Plasma Physics* (Kanazawa, Japan, 2018)

[42] F.L. Hinton and G.M. Staebler, Nucl. Fusion **29**, 405 (1989)

[43] T.N. Carlstrom, Fusion Sci. Technol. **48**, 997 (2005)

[44] X. Bonnin and W.L. Rowan, Nucl. Fusion **39**, 1009 (1999)

[45] S. Tsuji *et al.*, Nucl. Fusion **32**, 1313 (1992)

[46] A.V. Chankin *et al.*, Contrib. Plasma Phys. **40**, 288 (2000)

[47] J.G. Cordey *et al.*, Plasma Phys. Control. Fusion **38**, 1905 (1996)

[48] M. Barnes et al., Phys. Rev. Lett. **111**, 055005 (2013)

[49] J.P. Lee et al., Plasma Phys. Control. Fusion **57**, 125006 (2015)

[50] P.H. Diamond and Y.B. Kim, Phys. Fluids B **3**, 1626 (1991)

[51] W. Horton *et al.*, Phys. Fluids **30**, 3485 (1987)

[52] F. Wagner *et al.*, Phys. Rev. Lett. **49**, 1408 (1982)

[53] Y. Koide *et al.*, Phys. Rev. Lett. **72**, 3662 (1994)

[54] F.M. Levinton *et al.*, Phys. Rev. Lett. **75**, 4417 (1995)

[55] E.J. Strait *et al.*, Phys. Rev. Lett. **75**, 4421 (1995)

[56] X. Litaudon *et al.*, Plasma Phys. Control. Fusion **38**, 1603 (1996)

[57] E.J. Synakowski *et al.*, Phys. Plasmas **4**, 1736 (1997)

[58] C.M. Greenfield *et al.*, Phys. Plasmas **4**, 1596 (1997)

[59] F.X. Soldner and the JET Team, Plasma Phys. Control. Fusion **39**, B353 (1997)

[60] E.J. Synakowski, Plasma Phys. Control. Fusion **40**, 581 (1998)

[61] K.H. Burrell *et al.*, Plasma Phys. Control. Fusion **40**, 1585 (1998)

[62] Y. Koide and the JT-60U Team, Phys. Plasmas **4**, 1623 (1997)

[63] G.T. Hoang *et al.*, Nucl. Fusion **38**, 117 (1998)

[64] H.Y. Yuh *et al.*, Phys. Plasmas **16**, 056120 (2009)

[65] W. Horton, Rev. Mod. Phys. **71**, 735 (1999)

[66] T.S. Hahm, P.H. Diamond and E.-J. Kim, presented at *the 29th EPS Conference on Plasma Physics and Controlled Fusion* (Montreaux, Switzerland, 2002)

[67] J.C. Adam, W.M. Tang and P.H. Rutherford, Phys. Fluids **19**, 561 (1976)

[68] L. Chen *et al.*, Phys. Rev. Lett. **39**, 754 (1977)

[69] A. Rogister and G. Hasselberg, Phys. Fluids **26**, 1467 (1983)

[70] F.Y. Gang, P.H. Diamond and M.N. Rosenbluth, Phys. Fluids B **3**, 68 (1991)

[71] T.S. Hahm and W.M. Tang, Phys. Fluids B **3**, 989 (1991)

[72] J. Lang, S.E. Parker and Y. Chen, Phys. Plasmas **15**, 055907 (2008)

[73] Y. Xiao and Z. Lin, Phys. Rev. Lett. **103**, 085004 (2009)

[74] F. Merz and F. Jenko, Nucl. Fusion **50**, 054005 (2010)

[75] W.X. Wang *et al.*, Phys. Rev. Lett. **106**, 085001 (2011)

[76] B.H. Fong and T.S. Hahm, Phys. Plasmas **6**, 188 (1999)

[77] R.G. Littlejohn, Phys. Scr. **T2/1**, 119 (1982)

[78] T.S. Hahm, Phys. Plasmas **3**, 4658 (1996)

[79] T.S. Hahm, Lu Wang and J. Madsen, Phys. Plasmas **16**, 022305 (2009)

[80] N. Miyato *et al.*, J. Phys. Soc. Jpn. **78**, 104501 (2009)

[81] J.R. Cary and A.J. Brizard, Rev. Mod. Phys. **81**, 693 (2009)

[82] L. Wang and T.S. Hahm, Phys. Plasmas **16**, 062309 (2009)

[83] A.J. Brizard and F.X. Duthoit, Phys. Plasmas **21**, 052509 (2014)

[84] F.Y. Gang and P.H. Diamond, Phys. Fluids B **2**, 2976 (1990)

[85] Y. Idomura, S. Tokuda and Y. Kishimoto, J. Plasma Fusion Res. SERIES **6**, 17 (2004)

[86] L. Qi *et al.*, Phys. Plasmas **23**, 062513 (2016)

[87] P.H. Diamond *et al.*, in *Plasma Physics and Controlled Nuclear Fusion Research 1982* (IAEA, Vienna, 1983), Vol. I, p. 259

[88] G.J. Choi and T.S. Hahm, Nucl. Fusion **55**,093026 (2015)

[89] B.B. Kadomtsev and O.P. Pogutse, Sov. Phys. JETP **24**, 1172 (1967)

[90] Y. Kishimoto *et al.*, Plasma Phys. Control. Fusion **41**, A663 (1999)

[91] X. Garbet *et al.*, Phys. Plasmas **8**, 2793 (2001)

[92] S.V. Lebedev *et al.*, Plasma Phys. Control. Fusion **40**, 741 (1998)

[93] Y. Kamada *et al.*, Nucl. Fusion **39**, 1845 (1999)

[94] Y. Kamada, Plasma Phys. Control. Fusion **42**, A65 (2000)

[95] C.B. Forest *et al.*, Phys. Rev. Lett. **77**, 3141 (1996)

[96] G.D. Conway *et al.*, Phys. Rev. Lett. **84**, 1463 (2000)

[97] R.C. Wolf *et al.*, Nucl. Fusion **41**, 1259 (2001)

[98] G.D. Conway *et al.*, Plasma Phys. Control. Fusion **44**, 1167 (2002)

[99] T. Fujita *et al.*, Nucl. Fusion **38**, 207 (1998)

[100] M.G. Bell *et al.*, Plasma Phys. Control. Fusion **41**, A719 (1999)

[101] S. Ide *et al.*, Plasma Phys. Control. Fusion **44**, A137 (2002)

[102] C.M. Greenfield *et al.*, Nucl. Fusion **39**, 1723 (1999)

[103] T. Fujita *et al.*, Plasma Phys. Control. Fusion **46**, A35 (2004)

[104] E.J. Synakowski *et al.*, Phys. Rev. Lett. **78**, 2972 (1997)

[105] T. Fujita *et al.*, Phys. Rev. Lett. **78**, 2377 (1997)

[106] J.W. Connor and R.J. Hastie, Plasma Phys. **17**, 97 (1975)

[107] C.M. Roach, J.W. Connor and S. Janjua, Plasma Phys. Control. Fusion **37**, 679 (1995)

[108] C.M. Greenfield *et al.*, Phys. Plasmas **7**, 1959 (2000)

[109] J.E. Rice *et al.*, Phys. Rev. Lett. **111**, 125003 (2013)

[110] J.M. Kwon *et al.*, Nucl. Fusion **52**, 013004 (2012)

[111] J.P. Lee *et al.*, Phys. Plasmas **21**, 056106 (2014)

[112] H. Shirai *et al.*, Plasma Phys. Control. Fusion **42**, A109 (2000)

[113] Y. Sakamoto *et al.*, Nucl. Fusion **41**, 865 (2001)

[114] T.S. Hahm *et al.*, Plasma Phys. Control. Fusion **40**, 657 (1998)

[115] S.J. Wukitch *et al.*, Phys. Plasmas **9**, 2149 (2002)

[116] D.R. Ernst *et al.*, Phys. Plasmas **11**, 2637 (2004)

[117] D.R. Ernst *et al.*, Phys. Plasmas **16**, 055906 (2009)

[118] W.X. Wang *et al.*, Phys. Plasmas **14**, 072306 (2007)

[119] K. Ida *et al.*, Nucl. Fusion **55**, 013022 (2015)

[120] S. Yi *et al.*, Nucl. Fusion **55**, 092002 (2015)

[121] J.W. Heard *et al.*, Rev. Sci. Instrum. **70**, 1011 (1999)

[122] C. Sung *et al.*, Rev. Sci. Instrum. **83**, 10E311 (2012)

[123] G.S. Yun *et al.*, Rev. Sci. Instrum. **85**, 11D820 (2014)

[124] D. Eldon *et al.*, Rev. Sci. Instrum. **83**, 10E343 (2012)

[125] R.J. Hawryluk *et al.*, Nucl. Fusion **49**, 065012 (2009)

[126] T.E. Evans *et al.*, Phys. Rev. Lett. **92**, 235003 (2004)

[127] Y. Liang *et al.*, Phys. Rev. Lett. **98**, 265004 (2007)

[128] A. Kirk *et al.*, Nucl. Fusion **50**, 034008 (2010)

[129] J.M. Canik *et al.*, Nucl. Fusion **50**, 034012 (2010)

[130] W. Suttrop *et al.*, Phys. Rev. Lett. **106**, 225004 (2011)

[131] Y.M. Jeon *et al.*, Phys. Rev. Lett. **109**, 035004 (2012)

[132] B. Wan *et al.*, Nucl. Fusion **55**, 104015 (2015)

[133] P. Gohil *et al.*, Nucl. Fusion **51**, 103020 (2011)

[134] A. Kirk *et al.*, Plasma Phys. Control. Fusion **53**, 065011 (2011)

[135] S.M. Kaye *et al.*, Nucl. Fusion **51**, 113019 (2011)

[136] F. Ryter *et al.*, Nucl. Fusion **52**, 114014 (2012)

[137] W.-H. Ko *et al.*, presented at *the 26th IAEA Fusion Energy Conference, Kyoto,* EX/P4-4 (2016)

[138] P. Manz *et al.*, Phys. Plasmas **19**, 072311 (2012)

[139] L. Schmitz *et al.*, Nucl. Fusion **54**, 073012 (2014)

[140] M.N. Rosenbluth and F.L. Hinton, Phys. Rev. Lett. **80**, 724 (1998)

[141] H. Sugama and T.H. Watanabe, Phys. Rev. Lett. **94**, 115001 (2005)

[142] H. Sugama and T.H. Watanabe, Phys. Plasmas **13**, 012501 (2006)

[143] M. Leconte and P.H. Diamond, Phys. Plasmas **18**, 082309 (2011)

[144] M. Leconte and P.H. Diamond, Phys. Plasmas **19**, 055903 (2012)

[145] P.W. Terry *et al.*, Phys. Plasmas **20**, 112502 (2013)

[146] I. Holod *et al.*, Nucl. Fusion **57**, 016005 (2017)

[147] J.K. Park, *Ideal Perturbed Equilibria in Tokamaks*, Ph.D. Thesis, Princeton University (2009)

[148] Y. In *et al.*, Nucl. Fusion **55**, 043004 (2015)

[149] J.D. Callen, Nucl. Fusion **51**, 094026 (2011)

[150] Y. In *et al.*, Nucl. Fusion **57**, 116054 (2017)

[151] F.L. Hinton and M.N. Rosenbluth, Plasma Phys. Control. Fusion **41**, A653 (1999)

[152] W.W. Lee, Phys. Fluids **26**, 556 (1983)

[153] D.H.E. Dubin *et al.*, Phys. Fluids **26**, 3524 (1983)

[154] T.S. Hahm, Phys. Fluids **31**, 2670 (1988)

[155] J.K. Park *et al.*, Phys. Plasmas **16**, 056115 (2009)

[156] I.S. Gradshteyn and I.M. Ryzhik, *Table of Integrals, Series, and Products*, 7th edition, Academic Press, New York (2007)

[157] F.-X. Duthoit, A.J. Brizard and T.S. Hahm, Phys. Plasmas **21**, 122510 (2014)

[158] S.I. Braginskii, *Reviews of Plasma Physics* Vol 1, p 205, Consultants Bureau, New York (1965)

[159] S.W. Yoon *et al.*, Nucl. Fusion **51**, 113009 (2011)

[160] W.-H. Ko *et al.*, Nucl. Fusion **55**, 083013 (2015)

[161] Z. Lin *et al.*, Phys. Rev. Lett. **83**, 3645 (1999)

[162] M. Nunami, T.-H. Watanabe and H. Sugama, Phys. Plasmas **20**, 092307 (2013)

[163] Y. Xiao and Z. Lin, Phys. Rev. Lett. **103**, 085004 (2009)

[164] J.M. Kwon *et al.*, Comp. Phys. Comm. **215**, 81 (2017)

[165] M. Shimada *et al.*, Nucl. Fusion **47**, S1 (2007)

[166] W.-H. Ko *et al.*, presented at *the 59th APS-DPP meeting, Milwaukee, USA*, UP11.000544 (2017)

[167] S. Coda, M. Porkolab and K.H. Burrell, Phys. Rev. Lett. **86**, 4835 (2001)

[168] A Fujisawa *et al.*, Phys. Rev. Lett. **93**, 165002 (2004)

[169] A.D. Liu *et al.*, Phys. Rev. Lett. **103**, 095002 (2009)

[170] W.-H. Ko *et al.*, presented at *the 60th APS-DPP meeting, Portland, USA*, NO5.00003 (2018)

[171] J.D. Callen, Nucl. Fusion **51**, 094026 (2011)

[172] P.J. Catto and K.T. Tsang, Phys. Fluids **21**, 1381 (1978)

초록

이 논문은 토카막 수송 장벽 물리의 실용적 이슈들에 대한 설명을 제공하고자 하는 목적에서 E×B 흐름 층밀림 유도 난류 억제에 대한 이론적 확장을 수행한다. 첫째로, 기존 이론에서는 고려하지 않았으나 실제로는 빈번하게 관측되는 맴돌이의 초기 틀어짐을 고려하여 E×B 흐름 층밀림의 이 점 이론을 확장한다. E×B 층밀림과 초기 맴돌이 틀어짐의 상대적 방향이 E×B 층밀림 억제의 효율에 있어 중요한 요소임을 규명한다.

둘째로, 잡힌 전자 난류에 대한 적합한 이 점 방정식을 현대적 되튐운동론으로부터 체계적으로 유도한다. E×B 흐름과 자기 세차 표류를 함께 담고 있는 이 방정식은 과거 개별적으로 연구된 바 있는 E×B 층밀림 효과와 자기 세차 표류 층밀림 효과 간에 공동 작용이 존재함을 자연스럽게 드러낸다. E×B 층밀림과 자기 세차 층밀림 간의 상대적 부호가 공동 작용의 성격을 결정한다.

마지막으로, 공명 자기 섭동이 토카막의 구역 흐름에 미치는 영향을 선회운동론 방정식을 이용해 해석적으로 분석한다. 난류로부터 생성되는 E×B 흐름인 구역 흐름은 토카막 자기 구조에서 기인하는 무충돌적 감폭을 겪어 로젠블루스-힌튼 잔여 수준에 도달한다. 공명 자기 섭동이 도입된 경우 토카막의 구역 흐름은 이 잔여 수준으로부터 장기적 무충돌적 감쇠를 겪게 됨을 밝힌다.

위의 세 가지 이론적 확장들의 실험적 적용을 함께 논의한다. H-모드 전이 문턱의 위-아래 비대칭성, 전자 온도 내부 수송 장벽의 행동 양상, 공명 자기 섭동에 따른 H-모드 전이 문턱의 상승의 후보 기작들로서 본 논문의 이론연구 결과들을 제시하고 실험적 입증을 위한 방안을 논의한다.

주요어: 토카막, 난류, E×B 흐름 층밀림, 맴돌이 틀어짐, 자기 세차 표류, 공명 자기 섭동, 선회운동론, 되튐운동론

학번: 2012-23288

감사의 글

가장 먼저 지도교수 함택수 교수님께 존경과 감사를 표합니다. 교수님의 지도를 통해 미숙한 학생에서 전문적 연구자를 향해 성장할 수 있었습니다. 당신께서 몸소 가르쳐주신 핵융합 이론가로서의 견지와 자세는 저의 소중한 자산입니다. 조언과 따뜻한 격려로 힘을 더해 주신 황용석, 나용수, 정경재, 윤의성, 이정표 교수님께도 마음을 담아 감사 드립니다. 가까이에서 따스한 관심으로 지켜봐 주신 김곤호, 주한규, 김은희 교수님께도 깊은 감사를 드립니다. 언제나 맞아주시고 열정어린 도움을 주신 장호건, 권재민, 고원하, 강지성 박사님께도 감사를 전합니다.

학자의 길을 포기하지 않게 해준 친애하는 동욱형, 순우형에게 진심어린 감사를 표합니다. 앞으로도 서로 가까이 느끼며 버팀목이 되어주는 우정이 계속되길 바랍니다. 힘든 시기마다 어울려주고 위로와 격려로 힘이 되어준 상원형, 종인형, 현식형에게도 고마움을 표합니다. 정체의 위기마다 정반합의 발전을 함께 해준 유성형, 현석, 상균에게 특별한 감사를 전합니다. 지식을 나누는 즐거움을 알려준 남균형, 동현형, 민구형, 성무형, 철식형, 영기형, 영호, 재민, 찬영에게도 고마움을 전합니다. 같은 방을 함께 쓰면서 동고동락한 병훈형, 영우, 경표, 병준, 용직에게 격려를 전합니다. 모두의 앞길이 더욱 빛나길 기원합니다.

언제나 응원과 기도로 지탱해 주신 부모님께도 감사와 사랑을 전합니다. 앞으로도 건강하고 행복하시길 기원합니다. 마지막으로 짧은 공간에 미처 적지 못한, 지금까지 저와 함께 해준 모든 사람들에게 감사와 축복을 전하며 글을 마칩니다.